DOI: 10.1002/anie.201210009

Femtosecond Spectroscopy

From Single Hydrogen Bonds to Extended Hydrogen-Bond Wires: Low-Dimensional Model Systems for Vibrational Spectroscopy of Associated Liquids

*Martin Olschewski, Stephan Knop, Jörg Lindner, and Peter Vöhringer**

Keywords:
hydrogen bonds · IR spectroscopy · liquids · molecular dynamics · water

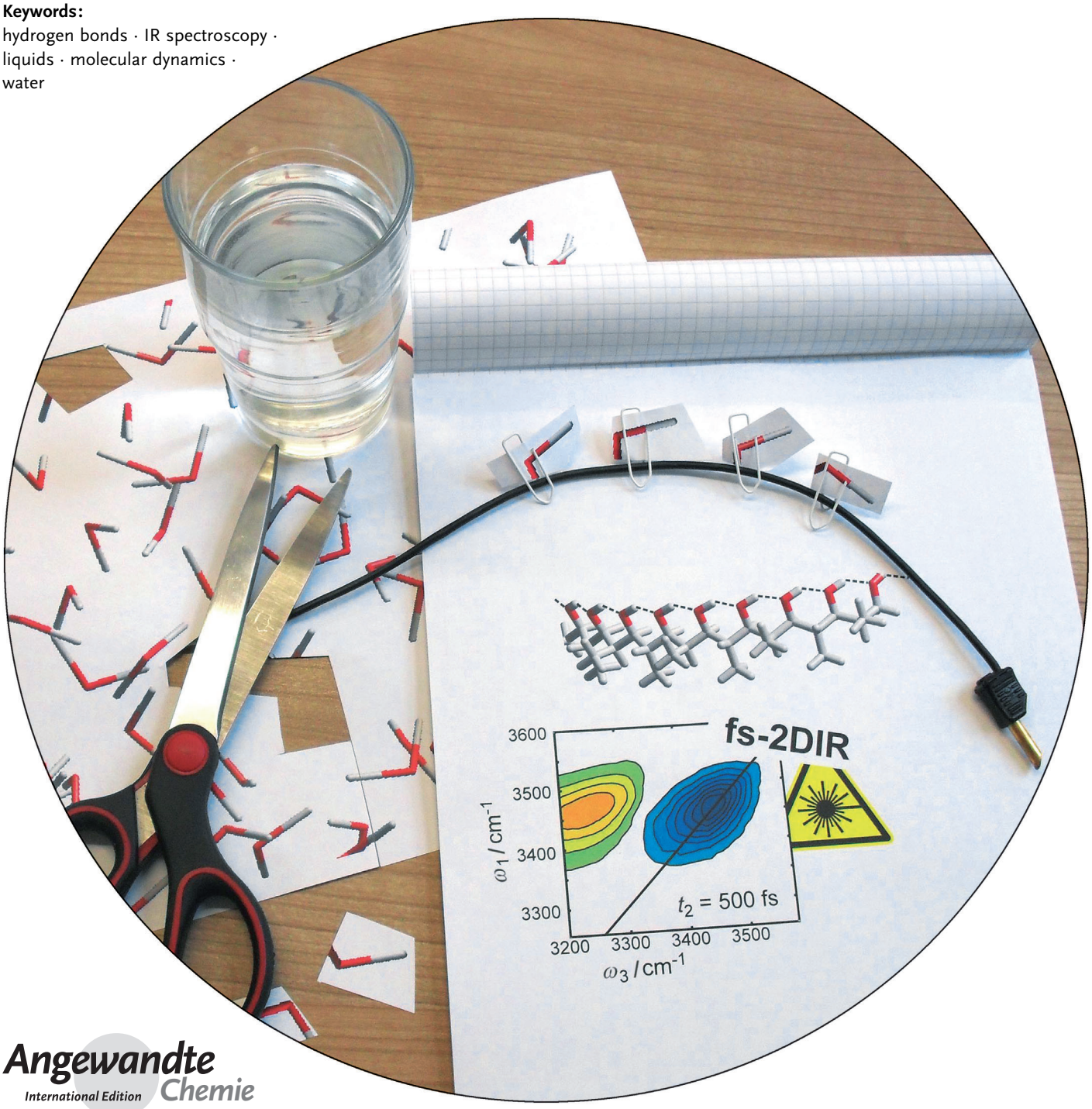

It is fair to say that if we ever wish to understand the anomalous properties of water, we need to study hydrogen bonds. Such a statement is based on statistical mechanics, which tells us how to calculate the structure and the thermodynamic properties of fluids and dense liquids from the forces between the particles. However, in the case of complex associated liquids, such calculations present a formidable—if not even insurmountable—challenge, which largely reflects our still-limited understanding of the hydrogen-bonding phenomenon itself. More experimental research on hydrogen-bonded systems is required to develop a comprehensive, satisfactory theory for associated liquids. This Review gives an introduction to the latest experimental technique currently being used to study the ultrafast structural dynamics of hydrogen bonds, namely two-dimensional infrared spectroscopy, and its applications to hydrogen-bonded systems of systematically increasing complexity, starting from the single hydrogen bond of a diol to low-dimensional extended networks of stereoselectively synthesized polyalcohols.

From the Contents

1. Introduction

In general, the structure and the dynamics of molecular liquids are the result of a complex interplay between thermal excitations of the particles and the interactions between them.[1] It is generally accepted that the short-range order of liquids, as revealed by X-ray and neutron scattering or by atomistic computer simulations, is largely the result of the repulsive forces between the molecules that arise from the exchange interaction of their electrons. In contrast, attractive forces, which may be due to dipole–dipole, dipole–induced-dipole, or dispersion interactions depending on the chemical structure of the molecular constituents of the system,[2] barely affect the particle packing and mostly serve to stabilize the liquid under the imposed thermodynamic conditions.[3]

The complexity is, however, substantially increased if there is a need to account for hydrogen bonding between the molecules.[4] This is because hydrogen bonding introduces highly specific and anisotropic interactions between pairs of particles containing light hydrogen atoms. As a consequence of the small mass of the proton, quantum effects may become important, which can only be taken care of properly in very demanding quantum-chemical/quantum dynamic treatments.[5] Alternatively, a plethora of empirical models and more sophisticated electronic structure calculations have been developed that can be used for highly efficient classical simulations of a wide variety of physicochemical properties for these associated liquids.[6] As a result of its directionality, hydrogen bonding furthermore introduces a peculiar short-range order that is not seen in simple non-associated liquids and that is responsible for their exceptional physical and chemical properties.

The most important associated liquid is unquestionably water.[7] Its O-O radial distribution function $g_{OO}(r)$ obtained either from experiment or from simulation uniquely shows that each H_2O molecule is embedded on average in a coordination environment composed of approximately four neighboring particles under ambient conditions.[8] This indicates an exceptionally open local structure and contrasts with the dense packing of simple atomic liquids with coordination numbers of roughly 12. In addition, the distance ratio between the first two maxima of $g_{OO}(r)$ of liquid water (2.73 Å/4.44 Å) is very close to the distance ratio between the first and second nearest neighbors in a diamond lattice, namely, $\sqrt{3/8} \approx 0.61$. These findings present unequivocal support for the existence of a hydrogen-bond network that retains much of the tetrahedral ordering that is characteristic of hexagonal ice (ice-Ih). The tendency of the H_2O molecule to coordinate four nearest neighbors in a tetrahedral fashion originates from its chemical structure, with two lone pairs of electrons enabling them to accept two hydrogen bonds while serving at the same time as a double hydrogen-bond donor.

As we will see later, hydrogen bonds are highly dynamic because they represent a rather weak type of interaction compared to ordinary covalent bonds. Hydrogen bonds can break and reform constantly as a result of thermal excitations. As a result of these structural rearrangements, the hydrogen-bond network loses the solidlike spatial periodicity and its formation becomes a short-range phenomenon that is random in both space and time. Therefore, only one more very weak maximum can be distinguished in $g_{OO}(r)$, which corresponds to the third nearest-neighbor peak around $r = 6.80$ Å, before

[*] M. Olschewski, S. Knop, Dr. J. Lindner, Prof. Dr. P. Vöhringer
Institut für Physikalische und Theoretische Chemie
Rheinische Friedrich-Wilhelms-Universität
Wegelerstrasse 12, 53115 Bonn (Deutschland)
E-mail: p.voehringer@uni-bonn.de
Homepage: http://www.chemie.uni-bonn.de/pctc/voehringer

all structural correlations are finally lost.[9] The structural rearrangements within the network are ultrafast in nature. From early studies on depolarized Rayleigh light scattering (DRS),[10] incoherent neutron scattering (INS),[11] and nuclear magnetic resonance (NMR)[12] it was concluded that these dynamics occur on a time scale of about 1 ps. The breakage and formation of hydrogen bonds is facilitated by the large amplitude of so-called librational degrees of freedom, which involve only pendulum-like motions of the light hydrogen atoms while the molecular centers-of-mass remain at rest. These unique intermolecular motions allow the network to respond quickly to moving charges[13] and dynamic charge redistributions,[14] thus making this liquid a unique medium for reactive chemical, biochemical, and electrochemical processes.

Since the structural dynamics associated with the hydrogen-bond network are so fast, their direct observation in the time domain is difficult. As powerful as they are, the experimental techniques mentioned above simply lack the necessary time resolution. DRS or INS can provide us with rich structural information, but only averaged over the long periods required to collect the scattering data. To obtain dynamical parameters, such as a hydrogen-bond lifetime, the scattering spectra have to be fitted to certain line-shape functions. Unfortunately, such results are valid only within the framework of the theory that justifies the used line-shape function and they are reliable only to the extent that the underlying theory is valid. Furthermore, neither of the above methods can reveal structure–dynamics correlations. It is actually quite important to know whether or not the lifetime of a hydrogen bond depends on its instantaneous configuration, for example, on its O–H···O bond length and bond angle. Thus, a method is required that has sufficient time resolution to capture hydrogen-bond dynamics and that provides us with a high sensitivity to the geometry of the hydrogen bond.

Time-resolved infrared (IR) spectroscopy with femtosecond (fs) laser pulses[15] is a method that perfectly fulfills these criteria. In the past, this technique has been shown to yield highly informative results regarding the various dynamical processes that can occur in liquid water or that can be induced in the liquid upon IR irradiation. Among such processes are fundamental molecular dynamics such as rotational diffusion,[16] vibrational energy relaxation[17] and redistribution,[18] excitation hopping,[19] vibrational spectral diffusion,[20] and hydrogen-bond breakage and formation.[21] These experiments have often been complemented by insightful molecular-level simulations.[22] Instead of touching upon all these aspects of aqueous dynamics, we refer at this point to excellent reviews in the recent literature.[23] Here, we wish instead to introduce the basic concepts of fs-IR laser spectroscopy and in particular its two-dimensional variant (2DIR)[24] for exploring hydrogen-bond dynamics in real time. As a consequence of the complexity of water, caused by the extension and the resultant spatially stochastic nature of its network, it is more instructive to focus on simple model systems featuring only a single or a few hydrogen bonds. This allows us to better reveal the spectrotemporal IR fingerprints of the various molecular dynamical processes that can simultaneously occur in such networks, regardless of their size and dimensionality.

Martin Olschewski studied Chemistry at the University of Bonn and received his diploma in 2009. His diploma thesis focused on the examination of vibrational energy relaxation of azide ions in liquid to supercritical water by time-resolved infrared pump-probe spectroscopy. He is currently carrying out PhD research centered on exploring hydrogen-bond dynamics in supramolecular systems using 2DIR spectroscopy.

Stephan Knop studied Mechanical Engineering and Chemistry in Aachen and Bonn. He received his diploma in 2009 for research on the vibrational dynamics in liquid amino alcohols. His PhD program was focused on unraveling the vibrational dynamics in extended hydrogen-bonded chains through 2DIR hole burning. He is now in the process of finalizing his PhD thesis and has already accepted an employment offer from Retsch Technology.

Jörg Lindner studied Physics at the University of Hannover where he received his PhD in 1990. In 1993, he went to JILA at the University of Colorado, Boulder, to work for two years as a postdoctoral fellow. From 1999 to 2004 he worked at the Biomolecular and Chemical Dynamics Group at the Max-Planck-Institute for biophysical Chemistry and since 2005 he has been a senior scientist at the Institut for Physical and Theoretical Chemistry at the University of Bonn.

Peter Vöhringer studied Chemistry at the University of Göttingen where he received his PhD in 1991. Following two years of postdoctoral work at the University of Pennsylvania, he joined the University of Karlsruhe, where he received his habilitation in Physical Chemistry in 1999. From 1998 to 2003 he was a research group leader at the MPI for biophysical Chemistry in Göttingen. In 2004 he became full professor of Physical Chemistry at the University of Bonn, where since 2011 he has also been the Spokesperson of the Collaborative Research Center "Chemistry at Spin Centers" of the German Research Foundation.

2. OH Vibrations as Probes for Hydrogen-Bond Structure and Dynamics

In a general hydrogen-donor/acceptor pair X-H···A, the intramolecular X-H stretching vibration can be used as a sensitive probe for the structure of the hydrogen bond. This is readily illustrated by a relatively simple quantum chemical calculation on one of the most primitive hydrogen-bonded model systems, the C_S-symmetrical open water dimer, $H_2O{\cdots}HOH$ (Figure 1 a).[25] In the following, we focus particularly on the triply deuterated water dimer, $D_2O{\cdots}HOD$, where the only remaining proton is exclusively involved in forming the hydrogen bond.[26] By analyzing this specific isotopomer, perturbations of the dimer's vibrational structure, which can occur in the OH stretching region because of the various couplings among the four hydroxy groups, are entirely suppressed. As a result, the hydroxy stretching vibration is the highest frequency mode of the system and it represents a true local mode.

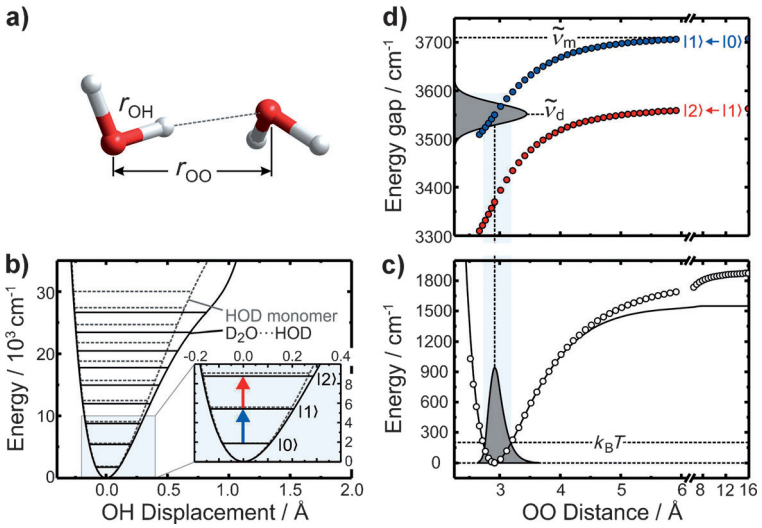

Figure 1. Results from an MP2 quantum chemical calculation of the water dimer. a) Optimized structure indicating the intramolecular OH distance r_{OH} and the intermolecular OO separation r_{OO}. b) Intramolecular OH stretching potential of the HOD monomer (dashed gray) and of the $D_2O{\cdots}HOD$ water dimer (black). The vibrational eigenstates are indicated as horizontal lines. c) Intermolecular OO stretching potential (circles) and fit to a Morse potential (solid curve). The gray area represents a thermal probability density at room temperature. d) Vibrational energy gaps corresponding to the fundamental (blue) and the first hot band (red) as a function of the intermolecular OO separation. The gray curve corresponds to the thermally broadened OH stretching infrared absorption spectrum.

At the level of theory used (RI-MP2/def2-TZVPP), the optimized structure features a nearly linear hydrogen bond with an O-H···O bend angle of 173°, an intermolecular O···O distance r_{OO} of 2.91 Å, and an intramolecular donor O-H distance r_{OH} of 0.965 Å. Next, we calculate the dimer's electronic energy as a function of the O-H displacement while retaining all other internal coordinates, thereby constructing the anharmonic OH stretching potential as shown in Figure 1 b. This allows us to identify in an adiabatic approximation the vibrational eigenstates as well as the vibrational transitions associated with the donor–hydrogen stretching vibration.[27] For comparison, the OH stretching potential and eigenstates of the HOD monomer in the absence of the hydrogen acceptor are calculated in a similar fashion. The fundamental OH stretching transition from $v=0$ to $v=1$ is found at 3550 cm^{-1} for the dimer, while that of the monomer is calculated to be 3706 cm^{-1}. Both numbers are in excellent agreement with experimental data.[28] Not only the fundamental transition but also all the corresponding overtones (e.g. $v=0$ to $v=2$) and hot transitions (e.g. $v=1$ to $v=2$) are shifted to lower frequencies relative to the monomer because of the hydrogen bonding. It can, furthermore, be noticed that the potential curve of the dimer is much more anharmonic than that of the monomer, thereby further enhancing the shift of the vibrational transitions to lower frequency.

This exquisite sensitivity of the donating hydroxy oscillator to the presence of a hydrogen acceptor can be understood in simple chemical terms and from the charge-transfer character of the hydrogen bond: as electron density is shifted from nonbonding orbitals located at the acceptor oxygen atom to antibonding orbitals of the hydroxy donor, the O–H bond is weakened, the potential along the OH distance is softened, and the OH frequency is decreased. For the water dimer, this interrelation can be formulated in a more quantitative fashion by computing a so-called relaxed scan of the full 12-dimensional potential energy surface of the system along the intermolecular O···O distance r_{OO} (Figure 1 c). Here, the (11) remaining nuclear degrees of freedom were allowed to geometrically relax so as to minimize the electronic energy at each preset value of r_{OO} while preserving the C_S symmetry of the dimer.

It can be seen that the motion along the O···O distance is bound as it experiences a restoring force (here, the binding energy of the hydrogen bond is 1875 cm^{-1} or, equivalently, 5.4 kcal mol^{-1}). The motion modulates the hydrogen-bond distance, which is why this degree of freedom could be labeled appropriately as the "hydrogen-bond stretching" vibration. Fitting a Morse potential to the computational data near the minimum yields an anharmonic frequency of 160 cm^{-1} for this mode. In the spirit of the adiabatic approximation, an OH local mode analysis can be carried out at each intermolecular separation, thereby providing us with full information regarding the dependence of the donor stretching vibrational manifold on the geometry of the hydrogen bond holding the two molecules together. Figure 1 d shows the energy gaps (in cm^{-1}) corresponding to the fundamental ($|1\rangle \leftarrow |0\rangle$) and the first hot ($|2\rangle \leftarrow |1\rangle$) transition of the anharmonic OH stretching vibration as a function of the O···O distance, which represents the anharmonic stretching vibration of the hydrogen bond.

It can be seen that the OH stretching fundamental $\tilde{\nu}_{OH}$ scales almost linearly with the O···O distance up to about 3.5 Å. Upon further increasing the intermolecular separation, the dependence of $\tilde{\nu}_{OH}$ on r_{OO} weakens to gradually approach

the spectral position of the OH stretching fundamental of the HOD monomer in the gas phase (3705 cm^{-1}). Similar calculations can also be carried out along other coordinates specifying the intermolecular configuration of the dimer, such as the in-plane and out-of-plane O···H-O bend angles. Again, motions along these coordinates are found to be weakly bound and could appropriately be referred to as "hydrogen-bond bending vibrations". As before, specific correlations exist between the intramolecular OH stretching transition frequency and the intermolecular bending coordinates specifying the geometry of the dimer.

So far, we have only discussed the connection between the OH stretching transition frequencies and the intermolecular configuration in terms of a quantum-chemical calculation on a simple water dimer at zero Kelvin. Such calculations have been tested in depth by extensive high-resolution spectroscopy on isolated hydrogen-bonded clusters in the gas phase.[29] Although we are far from treating bulk water, some fingerprints of the simple two-particle interactions considered so far will still be present in the vibrational spectra of its condensed phases. Firstly, the intermolecular degrees of freedom associated with a bending or a stretching of hydrogen bonds are indeed spectroscopically active. The calculations on the water dimer suggest that these are connected with vibrational wavenumbers around 200 cm^{-1} (6 THz). Thus, to observe these modes through light absorption, far-infrared[30] (terahertz) spectroscopy[31] needs to be conducted. Alternatively, low-frequency Raman scattering can also be performed to identify these nuclear degrees of freedom.[32]

Figure 2a displays the depolarized Raman spectrum of liquid water just above the freezing point, which was obtained by femtosecond optical Kerr effect (OKE) spectroscopy.[33] As a full time-domain technique, OKE is capable of entirely suppressing the elastic Rayleigh contribution and is, therefore, superior to frequency-domain light scattering for accurately measuring the line shapes of such low-frequency modes, in particular when the Raman cross-sections are small. The OKE spectrum of liquid water consists essentially of three, rather broad and almost structureless bands. A band

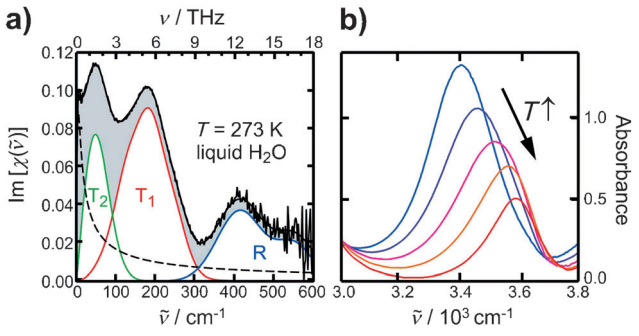

Figure 2. Vibrational spectra of liquid water. a) Intermolecular ("THz") spectrum of neat H_2O near the normal melting point obtained from Raman-induced optical Kerr effect spectroscopy. The spectrum is numerically decomposed into contributions originating from librational (R) and restricted translational (T_1 and T_2) degrees of freedom. b) Intramolecular spectrum in the OH stretching spectral region of HOD in liquid-to-supercritical heavy water at various temperatures.

(R) extending from 350 cm^{-1} to way beyond the free spectral range of the experiment of about 600 cm^{-1} originates from the librational degrees of freedom of the liquid (i.e., the rotational motion of the water particles that are hindered by hydrogen-bonded nearest neighbor molecules; also called "restricted rotation"). Another band (T_1) centered around 180 cm^{-1} is caused by the "restricted" translational motion of the water molecules in a direction parallel to the hydrogen bond. This degree of freedom leads to a periodic stretching and compression of the hydrogen bond and can thus be traced back to the elementary motion of the water dimer along the intermolecular distance r_{OO} discussed above. Finally, a third band (T_2) with a maximum at 49 cm^{-1} is observed which is also due to a restricted translation of the water molecules. However, here the translational motion is directed perpendicular to the hydrogen bonds and results in a deformation of the noncovalent contact. It is, therefore, related to the aforementioned bending of the hydrogen bond.

Whereas the intermolecular motions of the isolated water dimer are purely periodic, the equivalent motions in the dense liquid are heavily perturbed by interactions of the pairs of hydrogen-bonded molecules with other neighboring particles. Furthermore, the intermolecular degrees of freedom are highly collective in nature, involving not only motions of hydrogen-bonded pairs but also of larger structural entities whose spatial dimensions are comparable to the next-nearest neighbor O···O distance in the liquid.[32] By mimicking the condensed-phase system in terms of classical molecular dynamics and reducing the complex many-body forces to pairwise interactions only (a one-dimensional projection of which onto r_{OO} is shown in Figure 1c), the influence of thermal excitations on the vibrational spectra can be depicted as follows. Under ambient conditions, the thermal energy is roughly 200 cm^{-1}, which gives rise to a distribution of hydrogen-bond distances as indicated in Figure 1c by the gray shaded area. This in turn, translates into an approximately 100 cm^{-1} wide distribution of the OH stretching fundamental frequencies and, hence, to a broad OH stretching vibrational spectrum (see gray area in Figure 1d). Generally speaking, the very strong coupling between the intra- and intermolecular degrees of freedom associated with the hydrogen bond is reflected in 1) a very large shift to lower frequencies and 2) an enormous spectral broadening of the donor stretching resonance compared to the gas phase spectrum. Finally, because of the charge-transfer character of the hydrogen bond, the intensity of the OH stretching resonance in the infrared region is dramatically increased for the donor–acceptor complex compared to the isolated donor.

Switching now to the time domain: If we were able to follow a single water dimer (in an ensemble of such dimers) as a function of time, we would notice that it evolves along its intermolecular coordinates in a highly erratic fashion. In fact, the tagged pair performs a stochastic Brownian motion along r_{OO} as the other neighboring particles are intermittently pushing and pulling at the hydrogen bond, thereby randomly modulating the OH stretching potential of the donor, the O-H vibrational frequency, and the corresponding anharmonicity. This phenomenon is adequately termed "spectral diffusion" because the OH stretching resonance of the tagged dimer

performs stochastic excursions along the frequency axis as we continuously monitor it over time.

Having discussed the nature of the intermolecular degrees of freedom of hydrogen-bonded systems and their coupling to the high-frequency intramolecular stretching modes of the donor, we now turn our attention to the infrared absorption spectrum in the OH stretching region of monodeuterated water, HOD, highly diluted in liquid to supercritical heavy water, D_2O (Figure 2b). Under ambient conditions, the spectrum is maximal at 3400 cm^{-1} and hence, shifted to lower frequency by more than 300 cm^{-1} compared to the gas-phase spectrum. Its full width at half maximum is about 220 cm^{-1}. As the temperature is raised from about 300 K all the way up to 670 K, thereby entering the supercritical phase of the D_2O solvent, the spectrum loses intensity, it gradually shifts to higher frequencies, and the band narrows. These effects can be easily understood from Figure 1: upon heating the sample, the particle density diminishes and the average interparticle distance increases. Consequently, the absorption band shifts to higher frequencies as the density is decreased. Kandratsenka et al.[34] established a correlation between the OH stretching frequency and the mean nearest neighbor O···O distance for bulk liquid water that relies on experimental infrared spectroscopic data of HOD in liquid-to-supercritical D_2O, thereby essentially confirming frequency–structure correlations for water that were derived from various purely theoretical approaches.[20b,22d,f] However, even if such a frequency–structure correlation exists for a hydrogen-bonded system of interest, the linear absorption spectrum (as measured by a conventional FTIR spectrometer) gives us only an insight into the average structure and perhaps into the distribution of structures. To get a handle on the underlying thermally induced dynamics within this distribution of structures, that is, the structural dynamics of the hydrogen bond itself, we need to go beyond linear absorption spectroscopy. To this end, time-resolved two-dimensional spectroscopy (2DIR) with ultrafast infrared laser pulses has been developed and successfully applied to such problems over the last few years.

3. Two-Dimensional Infrared Spectroscopy

The basic ideas of 2DIR are as follows. Consider a molecular sample with an infrared OH stretching absorption band resulting from a broad inhomogeneous distribution of hydrogen-bonded geometries. With the term inhomogeneous, we refer to the notion that the individual OH oscillators do not suffer from spectral diffusion,[35] that is, their motion along the intermolecular coordinates is frozen out and, as a result, their individual frequencies are strictly temporally invariant. If a spectrally narrow laser pulse (called the "pump pulse", duration 300–500 fs), whose center frequency ν_{Pump} is tuned somewhere into this OH resonance, interacts with the sample, some of the molecules absorb the IR photons and are promoted to their first excited vibrational state ($v=1$). Notice, however, that only those molecules can absorb the photons whose OH-stretching fundamental falls within the bandwidth of the laser pulse. Therefore, and because of the frequency–structure correlation discussed above, the pump pulse photoselects from the broad distribution of hydrogen-bond geometries a rather narrow subensemble of molecules with fairly similar hydrogen-bond lengths and angles.[36] Since the vibrational ground state ($v=0$) of these photoselected molecules is now depleted, the sample features a diminished absorption at the frequency of excitation. Thus, if we measure the spectrum of the sample immediately after photon absorption, a dip (the "ground-state hole"[37]) is observed at the spectral position of the pump. The spectrum of the sample is measured with a second ultrashort infrared laser pulse (called the "probe pulse") whose bandwidth is ideally large enough to cover the entire linear absorption spectrum of the sample. In addition, the arrival time of the probe pulse at the sample can be adjusted in a variable fashion with respect to that of the pump. The experimental observable is then the pump-induced absorbance $\Delta OD(\nu_{Pump}, \nu_{Probe}, \tau)$, that is, the difference between the sample's optical density OD[38] in the presence and in the absence of the pump, as a function of the pump and probe frequencies as well as of the pump-probe time delay τ.

In this notation, the ground-state hole (i.e. the diminished $v=0\rightarrow1$ absorption) corresponds to a negative ΔOD. As the pump pulse also populates the first excited vibrational state of the OH stretching vibration, an additional signal corresponding to a negative ΔOD appears, which is due to the stimulated $v=1\rightarrow0$ emission and which is indistinguishable from the ground-state hole. Finally, a third signal with a positive sign exists that arises from the $v=1\rightarrow2$ excited-state absorption (ESA). This signal is markedly shifted to lower probe frequencies compared to the hole/emission because of the intrinsic anharmonicity of the vibrational mode being pumped and probed. The resultant total pump-induced absorbance is displayed schematically in Figure 3a as the

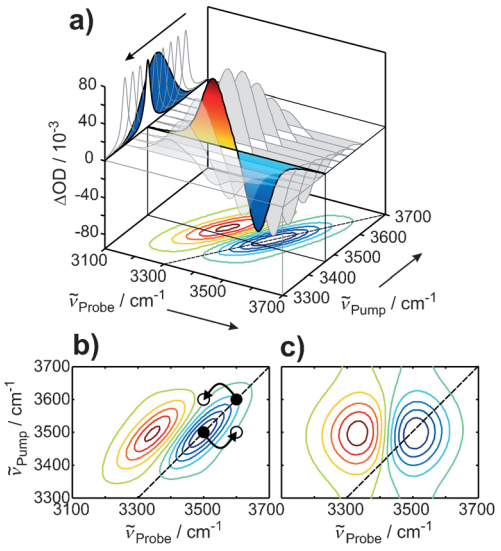

Figure 3. 2DIR spectroscopy. a) Collection of a series of infrared hole-burning spectra by tuning a narrow-band pump pulse through a vibrational resonance (see text for details). b, c) Contour representation of the 2DIR spectrum at early (b) and late (c) waiting times. Spectral diffusion randomizes the fundamental and transient absorption frequencies.

color-gradiented spectrum for a hypothetical absorption band centered at 3500 cm^{-1} (blue) and a representative pump pulse (white) that is tuned to the low frequency edge of the resonance. Basically, the complete 2DIR spectrum is then successively constructed by collecting a series of such pump-induced infrared spectra for a variety of slightly different center frequencies of the narrow-band pump pulse at a fixed pump-probe time delay. The full $\Delta OD(\nu_{Pump}, \nu_{Probe})$ surface is typically displayed as a contour representation, as shown in Figure 3a (bottom).

Since we have assumed an inhomogeneously broadened OH stretching absorption band resulting from a static distribution of intermolecular O-H···O distances and angles, the spectral position along the probe frequency axis of the ground-state hole and of the stimulated emission will strictly follow the frequency of the excitation. As a result, the 2DIR spectral contours will be elongated along the diagonal ($\nu_{Probe} = \nu_{Pump}$; Figure 3b). Provided the anharmonicity does not change across the absorption profile, the contours representing the $v = 1 \rightarrow 2$ excited-state absorption will feature the same tilt; they will, however, be shifted away from the diagonal because of the anharmonic character of the vibration. Moreover, the calculations on the water dimer and a careful inspection of Figure 1d already demonstrate uniquely that a gradually approaching hydrogen acceptor not only lowers the OH stretching frequency of the donor but it also increases its anharmonicity. Consequently, a greater than diagonal tilt should be observed for the anharmonically shifted absorption in the 2DIR spectra of inhomogeneous hydrogen-bonded systems.

So far, we have only discussed a 2DIR spectrum that is recorded immediately after absorption of the pump photon, that is, at a pump-probe delay of zero. But what happens if we wait for some time to elapse before recording the pump-induced absorbance, $\Delta OD(\nu_{Pump}, \nu_{Probe}, \tau > 0)$? The excess population created by the pump pulse in the $v = 1$ state must decay to recover the equilibrium distribution that existed prior to infrared excitation. Furthermore, what happens to the 2DIR spectrum if the fundamental frequencies of the individual OH oscillators changes with time, for example, because of thermal excitation and Brownian motion of the intermolecular O···O distance? In that case, the individual OH oscillators no longer retain their memory regarding the energy of the photon they absorbed at time zero.

Exploiting once more the frequency–structure correlation of the water dimer (Figure 1d), a given hydroxy group may be excited at time zero by a pump pulse that is centered at 3500 cm^{-1} because it is engaged in a hydrogen bond with the matching intermolecular separation of 2.65 Å. As a result of the thermal motion it might find itself at some later time engaged in a much longer hydrogen bond with an intermolecular separation of, for example, 3.20 Å. Hence, it will no longer be able to absorb a 3500 cm^{-1} photon because its OH stretching fundamental has responded to the different intermolecular configuration by adopting a $v = 0 \rightarrow 1$ energy gap of 3600 cm^{-1}. Provided this OH oscillator retains its vibrational excitation during the time period it will, therefore, contribute a stimulated emission signal (i.e. negative ΔOD) that is frequency-upshifted from the diagonal by 100 cm^{-1} along ν_{Probe} (Figure 3b). On the other hand, an oscillator that had a fundamental energy gap at time zero of 3600 cm^{-1} was unable to absorb the initial pump pulse. However, it might be able to absorb the probe light at that frequency a little later in time because it experienced a compression of the hydrogen bond, which down-shifted its OH stretching resonance by 100 cm^{-1} during the pump-probe time delay. This oscillator will, therefore, partially refill the hole that was initially burned by the pump at 3500 cm^{-1}.

In other words, the spectral diffusion associated with the hydrogen-bond dynamics homogenizes the OH stretching resonance with increasing pump-probe delay, thereby broadening the ground-state hole and making its spectral shape as well as position independent of the pump frequency. The same phenomenon is also seen in the spectral region of the $v = 1 \rightarrow 2$ excited-state absorption. As a consequence, the 2DIR contours evolve from being diagonally tilted at zero delay (indicating an inhomogeneous resonance, see Figure 3b) to vertically elongated at infinite delays (indicating a homogeneous resonance, see Figure 3c). The rate at which the diagonal tilt vanishes provides immediate and quantitative information regarding the dynamics of spectral diffusion and the loss of memory of the OH oscillators regarding their frequency of initial excitation.[39]

Superimposed on this dynamical evolution of the 2DIR line shape is a temporal decay of the amplitudes of both signal components, the ground-state hole/stimulated emission and the anharmonically shifted $v = 1 \rightarrow 2$ absorption. The decay is due to the finite lifetime of the $v = 1$ excited state and ultimately to the repopulation of the vibrational ground state that was initially depleted by the pump. The population relaxation is strongly dependent on the molecular system itself, on the details of its vibrational structure, and of course on the choice of the solvent.[40] What also appears highly intriguing about 2DIR spectroscopy is, therefore, its ability to unravel the lifetime of the $v = 1$ state (e.g. through the temporal decay of the $v = 1 \rightarrow 2$ absorption) as a function of the pump frequency and hence, as a function of the hydrogen-bond geometry that is photoselected by the pump, provided the infrared line shape is indeed broadened inhomogeneously at early delays.

During the last couple of years, 2DIR spectroscopy has advanced enormously in terms of theoretical understanding and instrumentation.[24b] The above "dynamic hole-burning" experiment that was originally developed by Hamm et al.[41] and that relies on tuning a narrow-band pump pulse through the linear absorption profile of the sample has the drawback of a relatively poor time resolution, as dictated by the Fourier theorem. To improve this aspect it is advantageous to replace the narrow-band (rather long) pump pulse by a coherent pair of much shorter broadband excitation pulses,[42] thereby providing a frequency comb for excitation whose fringe spacing is given by the reciprocal of the interpulse delay t_1. In such an approach, the time period t_2 between the second excitation pulse and the probe pulse adopts the role of the pump-probe delay of the hole-burning experiment and is often denoted "waiting time". Collecting with interferometric precision a set of pump-probe spectra for each interpulse

delay and subsequently Fourier transforming along t_1 retrieves the full 2DIR spectrum for a preset waiting time t_2. A detailed comparison between the two techniques, that is, 2DIR hole-burning versus Fourier-transform 2DIR spectroscopy, has been made by Cervetto et al.[43] A photograph displaying the 2DIR spectrometer at Bonn University is reproduced in Figure 4. It clearly highlights the instrumental complexity of this cutting-edge technique, and it demonstrates that there is still a long way to go before this powerful technique becomes a standard analytical tool in chemical research. Nevertheless, a first commercial spectrometer that is based on acousto-optic pulse shapers and that can be interfaced to ultrafast mid-infrared laser sources has recently become available.[44]

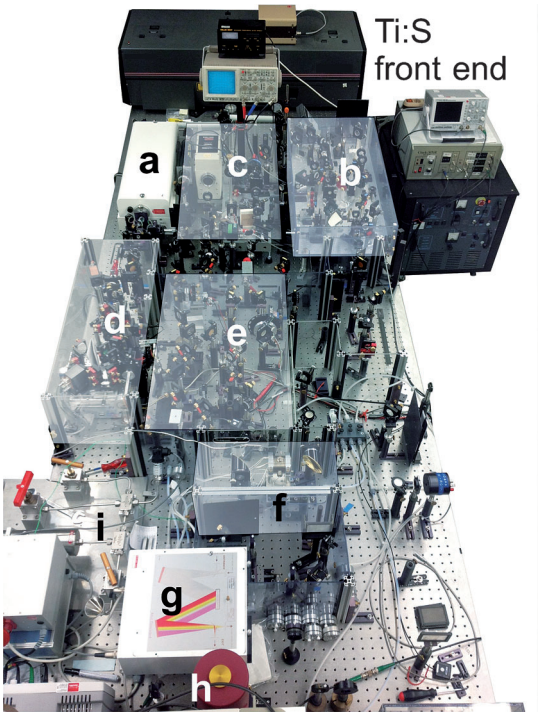

Figure 4. Fourier-transform fs-2DIR spectrometer. An ultrafast Ti:sapphire laser system synchronously pumps two independently tunable mid-infrared light sources (a and b). During operation, their pulse energies and spectra are continuously monitored by diagnostics (c). A Mach–Zehnder interferometer (d) generates a coherent pair of ultrashort pump pulses that can be variably delayed in (e) with respect to an ultrashort probe pulse. The three pulses are spatially overlapped in the sample (f). The probe pulse is spectrally dispersed in a grating monochromator (g) and its frequency-dependent intensity is measured by an array detector (h). The thermodynamic conditions of the sample (pressure and temperature) can also be independently controlled (i).

4. A Pair of Weakly Coupled Hydrogen-Bonded Hydroxy Groups

To better understand the influence of hydrogen bonding on the vibrational spectra of systems as complex as bulk liquid water, it is quite instructive to systematically increase the complexity of the hydrogen-bond network itself. Let us, therefore, begin with a simple hydrogen-bonded "dimer" of hydroxy oscillators. The noncovalent contact can be represented by the intramolecular hydrogen bond of a diol such as 1,8-dihydroxynaphthalene (DHN). To suppress any perturbing interactions of the system with the surroundings as much as possible, a nonpolar solvent such as carbon tetrachloride can be chosen. The FTIR spectrum in the stretching region of this compound and the structural data obtained from DFT calculations are displayed in Figure 5a,b, respectively. The

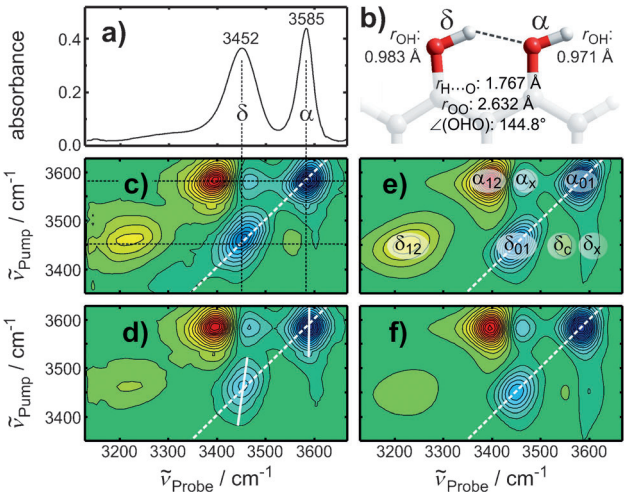

Figure 5. 2DIR spectroscopy of 1,8-dihydroxynaphthalene. a) Linear OH stretching absorption spectrum. b) DFT-optimized geometry and hydrogen-bonding structural parameters. c) and d) 2DIR spectra after 600 fs and 2.0 ps, respectively. e) and f) Corresponding simulated spectra and peak assignments.

molecular geometry of DHN is fully planar and the parameters of the inter-hydroxy configuration suggest a binding energy of the hydrogen bond that is similar to that of the water dimer. Indeed, at the DFT level RI-BP86/def2-TZVPP, the fully planar C_{2v}-symmetrical DHN conformer that features two free OH groups is roughly 2180 cm^{-1} higher in energy than the global minimum conformer shown in Figure 5b.

The FTIR spectrum consists of two well separated OH stretching bands: a rather narrow high-frequency band that originates from the hydrogen-accepting hydroxy group (denoted α-OH or "free" OH) and a broader band at lower frequencies that is undoubtedly due to the hydrogen-donating hydroxy group (δ-OH or "bound" OH). The shift to lower frequencies and the width of the δ band are fully in line with the above considerations on the water dimer. The 2DIR hole-burning spectrum at the earliest waiting delay of 600 fs is shown in Figure 5c. It displays two negative bands (α_{01} and δ_{01}) along the diagonal axis that correspond to the ground-state holes/stimulated emissions of the two oscillators α and δ. Spectrally downshifted by roughly 180 and 220 cm^{-1} along the probe axis, their corresponding excited-state absorptions (α_{12} and δ_{12}) appear as positive signals. All four peaks are significantly tilted toward the diagonal, thus indicating substantial inhomogeneous broadening and incomplete spectral-diffusive homogenization of the absorption band after 600 fs.

After 2.0 ps, the 2DIR spectrum has changed considerably (Figure 5d). Firstly, the diagonal elongation of the $v=0\rightarrow 1$ band of the free OH has completely vanished, while some small residual tilt of the corresponding band of the bound OH is still discernible. This indicates that the hydrogen-donating hydroxy oscillator suffers from different spectral diffusion dynamics than the free hydroxy group that serves as an acceptor. We can interpret this finding through a different reorientational mobility of the two OH moieties under thermal conditions. While the α-OH group can undergo quite a wide range of out-of-plane torsional excursions, the δ-OH group is conformationally locked by the hydrogen bond. Secondly, we notice that the amplitudes of both the hole/emission band and the excited-state absorption band of the bound hydroxy group have decayed relative to those of the free hydroxy group. Notice that the two spectra shown in Figure 5c,d are both normalized to the diagonal band of the α-OH. This observation clearly shows that the v = 1 state of the bound hydroxy group has a shorter lifetime than that of the free hydroxy group. Apparently, it seems as if hydrogen bonding accelerates the vibrational relaxation dynamics.

Most amazingly, another distinct and unexpected negative band (α_X) is observed upon pumping the free OH and probing near the bound OH (i.e. at $\nu_{Pump}=3585\ cm^{-1}$ and $\nu_{Probe}\approx 3460\ cm^{-1}$). An explanation for this prompt "cross" peak requires the two hydroxy oscillators to be mutually coupled and that they share a common vibrational ground state. In other words, exciting the α band depletes not only the v = 0 state of the acceptor but also that of the donor or, alternatively, the vibrational excitation of the α-OH is also experienced by the δ-OH. To be more quantitative, the magnitude of the coupling can also be estimated from quantum-chemical calculations. To this end the electronic energy $V(r_\alpha,r_\delta)$ of DHN is calculated in the vicinity of the equilibrium geometry as a function of the two OH bond distances r_α and r_δ. While the second derivatives $\partial^2V(r_\alpha,r_\delta)/\partial r_\alpha^2$ and $\partial^2V(r_\alpha,r_\delta)/\partial r_\delta^2$ are proportional to the square of the harmonic frequencies ν_α and ν_δ of the two local OH oscillators, the mixed partial derivative $\partial^2V(r_\alpha,r_\delta)/\partial r_\alpha\partial r_\alpha$ is proportional to their coupling β.[45,27] At the DFT level of theory stated above, we find an interaction energy of $-8\ cm^{-1}$ for the two OH stretching oscillators of DHN. In light of the total splitting of the two infrared bands of $133\ cm^{-1}$, this coupling is rather small and the two stretching vibrations should be considered as local modes. The interaction is, however, sufficient to slightly, but noticeably, delocalize the vibrational excitation and, thus, to give rise to this peculiar cross-peak.

The 2DIR spectra can be simulated within the framework of nonlinear response functions as developed by Mukamel[35] and by using the local mode description. This approach provides an intuitive interpretation of the individual diagonal and cross-peaks in terms of stretching anharmonicities Δ, as well as the various intermode couplings β. Since the interaction between the two OH oscillators is mutual, the question might be asked as to why the other cross-peak δ_x does not appear when the pump and probe frequencies are swapped. An inspection of the vibrational level scheme of DHN derived from such model simulations (Figure 6) reveals that

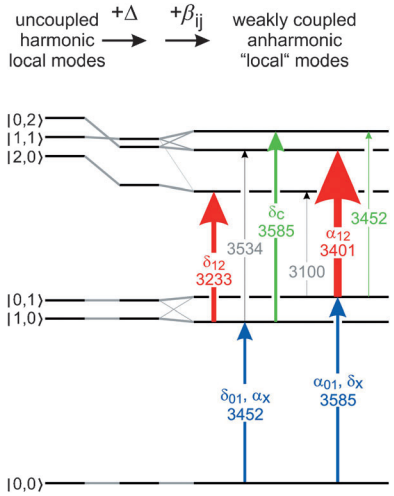

Figure 6. Vibrational level diagram of DHN in the local mode representation. Anharmonicities Δ of the bound and free local OH stretching modes and their mutual coupling β can be extracted from the 2DIR spectrum. The vertical arrows on the right indicate the various IR transitions between the fundamental and overtone levels. Their thickness symbolizes the squared magnitude of the corresponding transition dipoles and, hence, the 2DIR peak intensities. The numbers indicate transition wavenumbers in cm^{-1}.

this cross-peak is almost perfectly suppressed by an equally intense induced absorption (δ_C) arising from a transition of the lower one-quantum state (whose character is mostly "bound-OH fundamental") to the upper state of the two-quantum manifold (essential character of a fundamental excitation in each of the two oscillators).

The model simulations provide further, more quantitative information regarding the line-broadening dynamics as well as the vibrational relaxation dynamics. The random fluctuations of the vibrational energy gaps that give rise to spectral diffusion are usually treated as a stochastic Gauss–Markov process that is characterized by a correlation time τ_c and a mean-squared amplitude of the frequency excursions $\delta\nu^2$. For DHN, one finds that the bound OH oscillator retains its memory regarding the initial frequency of excitation for more than a picosecond ($\tau_c=1.4$ ps), while the free OH resonance is completely homogenized within a few hundred femtoseconds ($\tau_c=0.7$ ps). The vibrational lifetimes of the two oscillators are 0.7 ps and 6.4 ps for the bound and free OH groups, respectively.

5. A Pair of Fully Decoupled Hydrogen-Bonded Hydroxy Groups

The previous section has demonstrated that local OH stretching oscillators can be coupled and that their vibrational excitation can be partially delocalized. This intermode interaction exists even though the two vibrating bonds do not share a common atom, as is the case, for example, in monomeric water molecules, where this kinetic energy coupling contributes significantly to the splitting into symmetric and antisymmetric OH stretching fundamentals.[46] It

seems reasonable to assume that the contribution of the potential energy to the coupling depends on the relative alignment of the two hydrogen-bonded hydroxy groups and that we can actually tune this coupling by modifying the spatial configuration of the noncovalent contact.

The formation of a hydrogen bond is increasingly facilitated as the donor–acceptor distance decreases and as the angle between the two OH groups decreases. In DHN, these are almost perfectly parallel, spanning an angle of about 3°. In the closely related aromatic diol, 1,2-dihydroxybenzene (DHB or catechol), this angle is opened up to 54° (Figure 7),

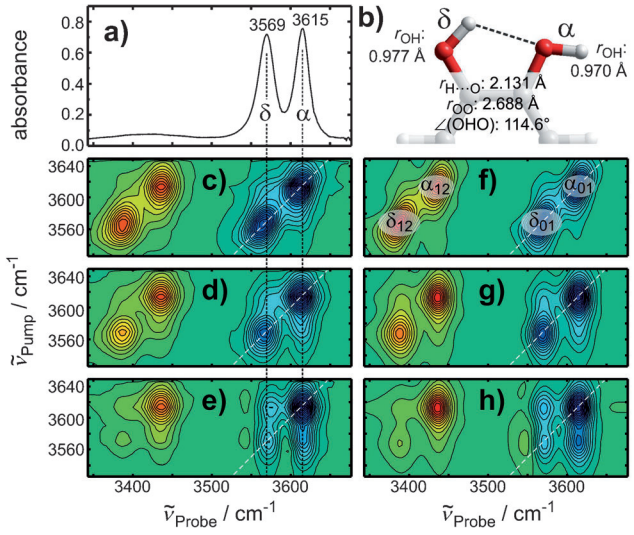

Figure 7. 2DIR spectroscopy of catechol. a) Linear OH stretching absorption spectrum. b) DFT-optimized geometry and hydrogen-bonding structural parameters. c)–e) 2DIR spectra after 600 fs, 3.0 ps, and 10.0 ps, respectively. f)–h) Corresponding simulated spectra based on a chemical exchange between bound and free OH groups.

thereby causing the O-H···O bend angle to decrease to about 115°. At the same time, the donor–acceptor separation as measured by the O···O and OH···O distances goes up dramatically. Compared to DHN, the weakened hydrogen bond of DHB is also reflected in a much shorter OH bond length of the donor and, consequently, in a much higher OH stretching frequency of the donor, as expected. This is fully confirmed upon inspection of its infrared spectrum. Once again, two absorption bands are observed; however, now the donor resonance is shifted to a higher frequency by more than 100 cm^{-1} relative to that of DHN. As a result, the donor–acceptor splitting becomes less than 50 cm^{-1}, thus indicating that the hydrogen-bonding interaction has indeed been enormously reduced. The question is now: what are the consequences of the modified donor–acceptor alignment for the 2DIR spectrum?

As shown in Figure 7c, the early time 2DIR spectrum features the expected diagonal peaks of the two types of oscillators. The bleaching/emission peaks (α_{01} and δ_{01}) appear at the proper fundamental frequencies, while the absorptive transitions to the two-quantum states (α_{12} and δ_{12}) appear anharmonically shifted to lower probe frequencies by about 180 cm^{-1}. The contours of all four signals are diagonally tilted. Most importantly, however, no prompt cross-peaks are discernible, thereby confirming that the two OH stretching oscillators are indeed fully decoupled. A DFT potential along the two local stretching coordinates further corroborates this conclusion. After 3 ps, the 2DIR spectrum has not changed by much, with the exception of the shapes of the contours, which have become more vertically elongated as a result of spectral diffusion (see Section 2). The 2DIR spectrum after 10 ps is, however, quite astonishing. Off-diagonal peaks, which were clearly absent at early times, now begin to show up (at $\nu_{Pump} = 3615$ cm^{-1}, $\nu_{Probe} = 3569$ cm^{-1}, and at $\nu_{Pump} = 3569$ cm^{-1} and $\nu_{Probe} = 3615$ cm^{-1}) and they even continue to increase relative to the diagonal peaks as the waiting time is further increased. Similar "delayed" cross-peaks are noticeable in the $\nu = 1 \rightarrow 2$ region, but because of the short lifetime of the δ-OH stretch, their intensity is heavily suppressed.

The origin of the delayed appearance of these cross-peaks needs to be clarified. Let us consider the "northwestern" cross-peak in the fundamental region: The diol is pumped at 3615 cm^{-1}, which depletes its vibrational ground state and gives rise to the diagonal peak at $\nu_{Probe} = 3615$ cm^{-1} where the vibrational excitation of the α-OH contributes a stimulated emission signal. An emission that peaks at the resonance of the δ-OH at $\nu_{Probe} = 3569$ cm^{-1} can only occur if the vibrational excitation is transferred during the waiting delay from the free OH stretch to the bound OH stretch. Likewise, the gradual appearance of the "southeastern" cross-peak signals that vibrational excitation is transferred in the opposite direction from the bound OH stretch pumped at 3569 cm^{-1} to the free OH stretch emitting at 3615 cm^{-1}. There are basically two distinctly different mechanisms that can account for the transfer of vibrational excitation from one mode to the other.

Referring to the vibrational manifold of the uncoupled anharmonic local modes shown in the energy level diagram of Figure 6, the two fundamental quanta of the α- and δ-OH (i.e. $|01>$ and $|10>$, respectively) are energetically very close. In fact, their energy gap is less than the thermal energy. A spontaneous uphill transition from $|10>$ to $|01>$ can occur if the required, but missing, energy is supplied by a low-frequency mode of the solvent or of the diol itself. In the first case, we speak of vibrational energy transfer (here, from the solvent to the solute) and in the second case, we speak of intramolecular vibrational energy redistribution. Similarly, a spontaneous downhill transition from $|01>$ to $|10>$ can occur if the released excess energy is absorbed by a low-frequency mode of the solvent or solute. This sort of energy relaxation does not occur immediately, but instead requires some finite time,[46a,b] which is why the intensity of the emissive and absorptive cross-peaks would grow with an increasing waiting delay.

An alternative mechanism is based on the relaxation of the molecular structure of the diol rather than on the relaxation of its vibrational energy. Imagine at time zero, the free OH stretching vibration is excited and we would detect its stimulated emission and ground-state hole exactly at the diagonal frequency. During a finite waiting time there is, however, the possibility that the hydrogen bond breaks and that the free OH converts into a bound OH. In turn, this process might cause the hydroxy group that initially served as

the hydrogen donor to transform into a new free hydroxy group. During this rearrangement, the hydrogen bond has reversed its direction and we, therefore, call it a hydrogen-bond reversal, or "flip-flop".[47] After the rearrangement, the hydroxy group that was initially excited at 3615 cm^{-1} as a free α-OH will now be seen in stimulated emission as a bound δ-OH at 3569 cm^{-1}, provided the vibrational lifetime of the α-OH is sufficiently long for the structural relaxation to occur. Of course, the reverse process of exciting an initial δ-OH and probing it as a final α-OH will also take place with equal probability. Apparently, the "flip-flop" process causes a spectral diffusion of the OH resonance between two discrete states namely, α-OH and δ-OH. Spectral diffusion occurring in such a discrete basis of states is also called "chemical exchange".

Whether or not such a structural "flip-flop" isomerization is at all possible depends on the topology of the multidimensional potential energy surface (PES) of the diol. There are essentially only two nuclear degrees of freedom that are of particular relevance for the hydrogen-bond reversal of catechol. These are the two CC-OH torsions, and considering that the CCO and COH bend angles never deviate much from their equilibrium values, they uniquely define the relative angular orientation of the two OH groups.

Figure 8a displays the potential energy of catechol as a function of these two dihedral angles θ_1 and θ_2 (level of theory RI-BP/def2-TZVPP). The PES is a highly complex, corrugated landscape with numerous minima and maxima. For $\theta_1 = 180°$ and $\theta_2 = 0°$, the molecule assumes its global minimum structure **1**, which we assign (arbitrarily) to a right-to-left-oriented hydrogen bond in Figure 8b. For $\theta_1 = 180°$ and $\theta_2 = 180°$, the two OH dipoles point in opposite directions and the hydrogen-bond interaction between them is fully eliminated. Nevertheless, the fully planar structure (not shown) having two free hydroxy groups at the same time corresponds to a local PES minimum, which is energetically higher by about 3.9 kcal mol^{-1} (or equivalently, 1350 cm^{-1}) than structure **1**. Nonplanar structures with two free OH groups are inherently unstable and they give rise to very high energy barriers of about 11.5 kcal mol^{-1} (approximately 4000 cm^{-1}).

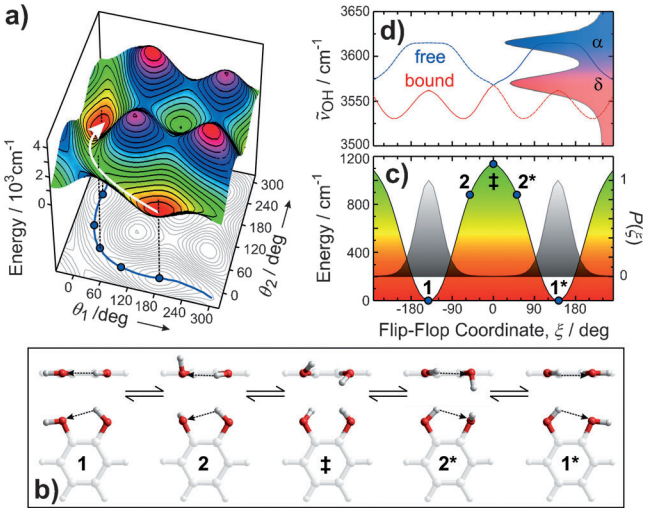

Figure 8. Hydrogen-bond flip-flop in catechol. a) Potential energy surface relevant to hydrogen-bond reversal from DFT calculations. b) Snapshots of catechol along the flip-flop coordinate. c) One-dimensional cut through the surface along the flip-flip coordinate and classical Boltzmann density P(ξ) (gray). d) Instantaneous OH stretching frequency as a function of the flip-flop coordinate and mapping onto the linear absorption spectrum.

What is most intriguing about the PES is a rather deep valley that interconnects right-to-left hydrogen-bonded configurations such as **1** with those that have a left-to-right oriented hydrogen bond such as **1*** (Figure 8b). The latter structure is energetically degenerate with **1** and emerges from it by simply swapping the two dihedral angles θ_1 and θ_2. These two otherwise identical configurations are separated by a true saddle point on the multidimensional PES (i.e. by a transition-state structure ‡) at $\theta_‡ = \theta_1 = \theta_2 = 37.5°$. A motion of the molecule in the vicinity of the saddle point that is directed along the bisector $\theta_1 = \theta_2$ can be described as a conrotatory dual CC-OH torsional isomerization in which the two hydroxy groups rotate synchronously and in the same sense (e.g. both clockwise or counterclockwise). A motion near the saddle point that occurs perpendicular to the bisector, that is, $\theta_1 = 2\theta_‡ - \theta_2$, is equivalent to a disrotatory dual CC-OH torsional isomerization, where the synchronous rotation of the two OH groups occurs in the opposite sense (i.e. one OH turns clockwise and the other one counterclockwise).

The minimum energy path within this valley constitutes the reaction coordinate ξ for the hydrogen-bond flip-flop and it is highlighted in the full PES by the white arrow. A one-dimensional cut through the PES along the flip-flop coordinate is presented in Figure 8c together with the Boltzmann density at room temperature. In this representation, the PES reduces to a simple double-well potential and the transition state projects onto the peak of an intermediate barrier. After correction for the zero-point energy, the threshold for the hydrogen-bond reversal along the flip-flop coordinate amounts to a mere $E_0 = 3.0$ kcal mol^{-1} (or equivalently, 1000 cm^{-1}), thus suggesting that the system is fully fluxional at room temperature.

To test this notion, we calculate a thermal rate constant $k_{TST}(T)$ by using canonical transition-state theory (TST).[48] To this end, we conduct a normal mode analysis of the optimized structure as well as of the transition state. This provides us with their harmonic frequencies, which we need to compute the vibrational partition functions Q_1 and $Q_‡$ of structures **1** and ‡. From Equation (1), where k_B is Boltzmann's constant, h is Planck's constant, and T is the temperature, and realizing that for symmetry reasons the forward and backward rates are equal, we obtain a characteristic time $\tau_{ex} = 1/2\,k_{TST}(T)$ of 22 ps at 300 K between left-to-right- and right-to-left-oriented hydrogen bonds.

$$k_{TST}(T) = (k_B T/h)\,(Q_1/Q_‡)\exp(-E_0/k_B T) \qquad (1)$$

Furthermore, the motions along the flip-flop coordinate strongly couple to the two OH stretching vibrations of catechol. This is demonstrated by performing at a vibrational analysis of the instantaneous geometry of the molecule at every value of ξ (Figure 8d). Deep in the potential wells, the

hydroxy stretches are fully decoupled and they are best described as local modes. In contrast, directly at the barrier top, the two OH oscillators become symmetry-degenerate and any finite coupling between them fully delocalizes the vibrations such that they are best described as symmetric and antisymmetric normal modes of the transition state. Most importantly, the unique interrelation between the OH stretching frequency and the instantaneous geometry of the molecule along the flip-flop coordinate is responsible for spectral diffusion and vibrational line broadening, as well as for a dynamical exchange between the OH stretching vibrational resonances of free and bound OH groups by virtue of the hydrogen-bond flip-flop dynamics.

Finally, to extract a rate constant for the exchange dynamics from the experimental 2DIR data, the nonlinear response function formalism can be employed again together with a simple kinetic model that describes the interconversion between the two structures with oppositely oriented hydrogen bonds (Figure 7 f–h). The simulations retrieve an exchange time of 19 ps, which is indeed in excellent agreement with the ab initio rate constant derived from TST and the DFT potential. Altogether, the data on catechol displayed in Figures 7 and 8 represent a very nice example of the utility of 2DIR spectroscopy as an ultrafast laser-based variant of chemical-exchange spectroscopy,[49] which was established a long time ago in the context of nuclear magnetic resonance.[50]

We close this section by drawing the analogy of the flip-flop motion of catechol to the disrotatory in-plane hydrogen-bond exchange motion of the hydrogen fluoride dimer, which has been analyzed in great detail in terms of tunneling splittings by Quack and Suhm.[51]

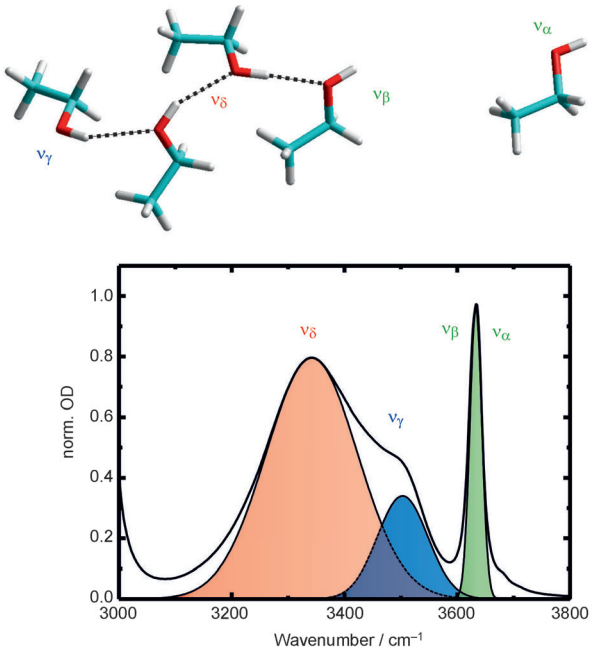

Figure 9. FTIR spectrum of a 0.2 M solution of ethanol in carbon tetrachloride. Various types of hydroxy groups of ethanol monomers and oligomers contribute to the OH stretching region of the spectrum.

6. Extended Chains of Hydroxy Groups

So far, we have only discussed systems with isolated hydrogen bonds. In nature, hydrogen bonding is often a cooperative phenomenon that leads to the formation of extended networks such as in liquid water or in ice. To systematically study the effects of such a network formation on the vibrational dynamics of OH stretching oscillators, various research groups have studied oligomeric alcohol clusters dissolved in nonpolar liquids.[52] In particular, for concentrations above 0.05 M, ethanol forms hydrogen-bonded chains and rings in carbon tetrachloride solution. As shown in Figure 9, the aggregation can easily be verified in the infrared spectrum, where different types of hydroxy groups can be distinguished. The OH groups of residual monomers (α) and OH groups of aggregates that dangle into the nonpolar solvent (β) give rise to a very sharp band at 3620 cm^{-1}. A weaker, slightly lower frequency band centered at 3500 cm^{-1} is typically assigned to hydroxy groups that terminate chain aggregates as hydrogen donors (γ). The most prominent band has a maximum around 3320 cm^{-1} and is assigned to OH groups (δ) that serve as both hydrogen donors and acceptors in the interior of the aggregates.

Research on these clusters has mostly focused on the dynamics of vibrational relaxation following an initial fundamental OH stretching excitation.[52d–g] Lifetimes below 1 ps were found and a vibrational predissociation was proposed as the relaxation mechanism (see below). A particular complication arises in oligomeric alcohols in nonpolar solvents from the fact that an excited OH stretching oscillator is always in spatial proximity with other non-excited oscillators. Moreover, excited and non-excited hydroxy groups may experience very similar hydrogen-bond configurations. As a result, their OH stretching fundamental energy gaps may become instantaneously degenerate, whereupon the vibrational excitation can very quickly hop from one molecule to another. Such a resonant transfer of vibrational energy is dipole-induced (just like in Förster's resonant transfer of electronic energy) and leads to a rapid loss of memory regarding the frequency of the initial excitation.[52d,19] Furthermore, we have already seen that OH stretching excitations can be (partially) delocalized over two OH groups of a single molecule, provided the intramolecular hydrogen-bond configuration gives rise to a considerable coupling between the two local modes. The question may then be raised as to whether the OH stretching vibrations of intermolecular aggregates are actually strictly localized on an individual molecule or already delocalized over many particles.[17d,18a,22n,o,53a–c] Lastly, the system of alcohol oligomers is stoichiometrically not well defined and it is impossible to distinguish between the various clusters of different sizes. In addition, cyclic aggregates coexist with chain oligomers, neither of which can be uniquely discriminated. Therefore, molecular systems would be ideal that allow for full control over the size of the hydrogen-bond network (i.e. the number of hydroxy moieties) as well as over the network dimensionality (i.e. one-dimensional wires, two-dimensional rings or grids, or full three-dimensional meshes).

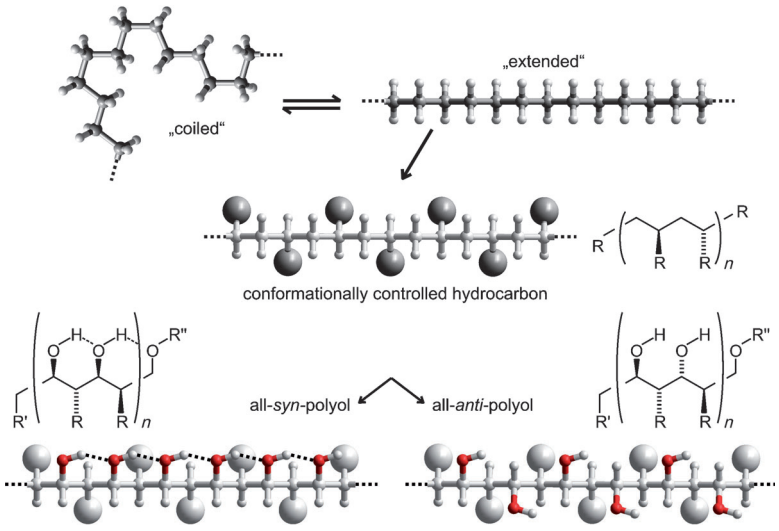

Figure 10. Paterson-type arrays of hydroxy groups (OH wires) can be understood as saturated hydrocarbons that are guided into an extended linear-chain conformation through a repetitive 1,3-*anti*-methylation pattern. A simultaneous 1,3-*syn*-hydroxylation favors the formation of a collective hydrogen-bond network, whereas a 1,3-*anti*-hydroxylation inhibits the formation of such a network. For simplicity, methyl groups are depicted as gray balls. The residues R' and R'' represent a methyl and a benzyl group, respectively.

Paterson and Scott[54] developed an iterative, boron-mediated aldol-based strategy to assemble extended polypropionates, such as those shown schematically in Figure 10. For our purposes, the molecules can be thought of as saturated hydrocarbons bearing a stereoregular 1,3-*anti*-methylation pattern. The repulsive interactions between the bulky methyl substituents are responsible for a strong propensity of the alkanes to adopt an extended linear-chain conformation rather than a randomly coiled conformation, which would otherwise prevail under ambient conditions.

We imagine for a moment all of the C atoms of the stretched alkane backbone to be lying in a plane perpendicular to the paper plane. Hydroxy groups are now attached to every remaining carbon atom along the alkane chain in either a 1,3-*syn* or a 1,3-*anti* arrangement. In the former case, all the hydroxy groups are located on the same side of the backbone plane and are, therefore, oriented favorably for formation of an extended hydrogen-bond network. In contrast, in the latter case, alternating hydroxy moieties are located on opposite sides of the backbone plane and consequently, a network formation is expected to be strongly inhibited. Paterson and Scott carried out NMR spectroscopic studies to test for the presence of hydrogen-bonding interactions in these systems.[54] Each hydroxy proton of an all-*syn*-polyol was found as a distinct and well-separated singlet, thereby fully confirming the existence of a well-defined unique intramolecular hydrogen-bond network. In other words, each hydroxy proton experiences its own characteristic chemical environment that is stable on the NMR time scale. Quite in contrast, all the OH protons of the all-*anti*-polyols collapse into a single NMR signal, which indicates that such a well-defined and stable network does not exist in these diastereomers.

The DFT-optimized structures (RI-BP86/def2-TZVPP) for the homologous series of Paterson's all-*syn*-polypropionates are displayed in Figure 11. As an example, let us discuss the tetrol structure (b) in more detail. All four hydrogen-bonded contacts are very similar, with a very short O···O distance of (2.65 ± 0.06) Å, that is, similar to DHN. In addition, adjacent OH bonds are neatly lined up and span angles of 8°, 15°, and 18°. A slight curvature of the hydrogen-bonded array is likely to reflect some residual dispersion interaction between 1,5-*syn*-oriented methyl groups. The oxygen atom of the benzyl ether residue (a leftover of the chemical synthesis) serves as a terminal hydrogen acceptor such that a free OH group is prevented. Scanning along the four local OH stretching coordinates provides harmonic local ("site") frequencies of 3481 cm^{-1}, 3463 cm^{-1}, 3423 cm^{-1}, and 3482 cm^{-1}. Furthermore, nearest neighbor intermode couplings of $-(20\pm2)$ cm^{-1} are obtained and there is even a significant next-nearest neighbor coupling of -3 cm^{-1}. Thus, and in contrast to DHN, the magnitude of the interaction between the modes is similar to the difference in their site frequencies and we can expect the formation of more delocalized excitations such that the OH stretching vibrations of the tetrol can also be suitably described as collective normal modes.[55]

The results of a normal mode analysis are compiled in Figure 12 (upper panels). Once again focusing on the tetrol, the lowest frequency normal mode arises when all four OH oscillators move periodically in phase. It has a frequency of

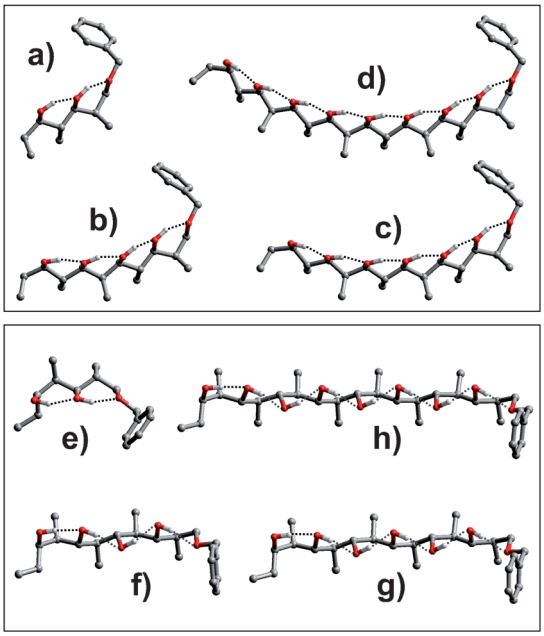

Figure 11. DFT-optimized structures of the series of all-*syn*- (top) and all-*anti*-polypropionates (bottom): diol (a,e), tetrol (b,f), hexol (c,g), and octol (d,h). Note, the octols have not been synthesized yet. All hydrogen atoms except hydroxy hydrogen atoms are removed for clarity.

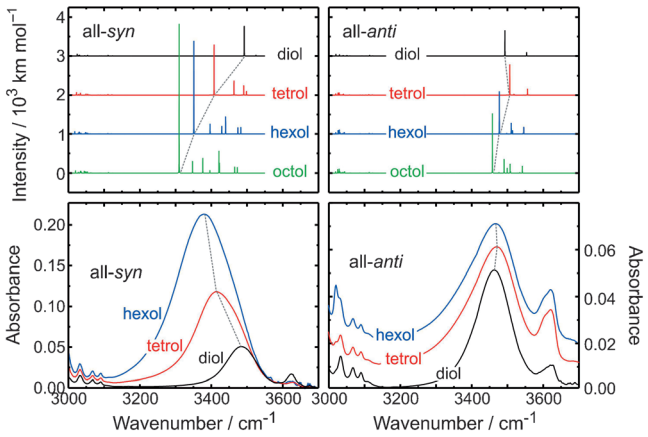

Figure 12. Normal-mode analysis of the stereoselectively synthesized polyalcohols and their FTIR spectra in nonpolar liquid solution at room temperature. Note the continuous spectral shift of the band with increasing chain length of the all-*syn* species, which is absent in the all-*anti* diastereomers.

3407 cm^{-1} and carries most of the infrared oscillator strength. In contrast, the highest frequency mode is formed when the four OH vibrators move periodically out of phase. It has a frequency of 3494 cm^{-1} and is only weakly IR active. What we are phenomenologically describing here is basically a linear chain of coupled oscillators, and the physics of the chain excitations is highly reminiscent of exciton states of coupled electronic chromophores[56] such as in Scheibe's J-aggregates or in chlorophyll assemblies of photosynthetic pigments.[57] It is not at all unreasonable to label the above all-*syn*-polyols as "V-aggregates" or "vibrational aggregates".[58] However, the mechanism of the coupling in electronic aggregates is pure transition dipole–dipole interaction between optical chromophores, whereas in our chains of hydroxy groups there is hydrogen bonding in addition to dipole–dipole coupling between the infrared chromophores (i.e. the OH oscillators). In the point-dipole approximation, the strength of the dipole–dipole coupling scales with the inverse cube of the distance and depends on the relative angular orientation between the two interacting units.[57] One speaks of vibrational excitons (a term originating from solid-state physics)[59] when the assumption is made that the dipole–dipole coupling mechanism suffices to describe the interaction between spatially nearby hydroxy oscillators. In the context of 2DIR spectroscopy, such a model has been originally introduced to describe the vibrational excitations of coupled carbonyl groups in extended peptide chains.[41,60] In the context of hydrogen-bonded Paterson-type chains of hydroxy oscillators, the quality of the exciton model has also been assessed recently by using geometrical parameters of the chain from DFT calculations.[55b] It turns out that the dipole–dipole interaction energy can account for about 50–70% of the coupling between hydrogen-bonded OH groups in the stereoselectively synthesized linear OH arrays. The exciton model is also very well developed for numerical simulations of the OH vibrational spectroscopy of liquid water.[22n,o,53a–c]

The presence of thermal excitations will lead to fluctuations of the structure of the linear chain, which in turn will translate into fluctuations of the OH "site" frequencies and into fluctuations of the intermode couplings. To get an idea of the structural variations of such systems under ambient conditions, one can carry out classical molecular dynamics (MD) simulations. Representative slices of dynamical trajectories obtained from such computer experiments (Langevin-MD, AMBER) are shown in Figure 13 for the all-*syn*- (left column) and for the all-*anti*-tetrol (right column). It must be emphasized that there are actually more than 120 different backbone conformations of the all-*anti* diastereomer that lie within an energy of 6 kcal mol^{-1} in the classical force field. Structural transitions between different backbone conformers occur on a time scale of about 1 ns and are, therefore, slow compared to fluctuations of the relative orientations of the hydroxy groups defining the hydrogen-bond network. Therefore, Figure 10 compares two MD trajectories where the polyol backbone was fully extended.

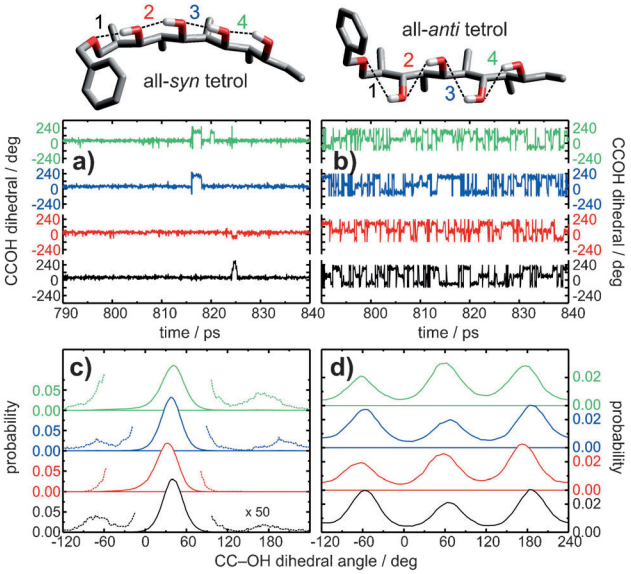

Figure 13. Time slices of Langevin molecular dynamics trajectories of the all-*syn*- (left column) and all-*anti*-tetrols (right column). The simulation temperature was 300 K and the friction coefficient was 0.1 ps. a) and b) Time-dependent torsional angles. c) and d) Torsional probability distributions.

Figure 13 a,b display the four CC-OH torsional angles as a function of time. Since the motion along the backbone torsions is slow on the 50 ps window of the time slice, the set of angles gives a quick overview of the relative alignment of the OH moieties in the network. In particular, for the all-*syn* diastereomer, when two hydroxy groups are parallel to each other, their corresponding dihedral angles are similar and the hydrogen bond between them is fully formed. In contrast, when they point in opposite directions the two CC-OH torsions differ by about 180° and the hydrogen bond is broken. Whenever all four dihedral angles are similar, the entire network is intact. The MD simulations demonstrate that the all-*syn*-polypropionates undergo mostly fluctuations with small amplitudes and that breakage of the hydrogen bond is a relatively rare event. In the time slice shown in

Figure 13a, such occasional events can be observed from 816 ps onwards where initially the two OH groups 3 and 4 (Figure 13 for the numbering convention) suffer from a spontaneous hydrogen-bond flip-flop, thereby breaking the noncovalent contact between OH-2 and OH-3. Within 2 ps, the full network is re-established, but after another 2 ps the terminal hydroxy group reorients by approximately 160°, thus cleaving the hydrogen bond between OH-3 and OH-4 over a time period of about 700 fs. Around 825 ps, another network disruption can be observed involving OH-1 (and to some extent also OH-2) and lasting for about 800 fs.

Inspecting the complementary time slice for the extended conformer of the all-*anti*-tetrol (Figure 13b), we note that the fluctuations are of much larger amplitude and occur extremely rapidly compared to the all-*syn* diastereomer. Indeed CC-OH torsional transitions occur multiple times in a period as short as 1 ps, thus indicating that the hydrogen bonds are very weak, that they are highly fluxional and that their lifetime is shorter than 500 fs. A numerical analysis of these trajectories yields, for example, probability distributions along the torsional degrees of freedoms as exemplified for the two tetrols in Figure 13c,d. From these one can easily extract CC-OH torsional free energy landscapes. The MD simulations are fully in line with the NMR results. They confirm that the all-*syn*-polypropionates adopt unique structures exhibiting an extended hydrogen-bond network that is stable on a nanosecond timescale, whereas their all-*anti* counterparts are highly fluxional within the CC-OH torsional potentials such that a structurally well-defined hydrogen-bond network cannot be identified. Furthermore, whereas the all-*syn*-polyols strongly prefer a stretched backbone conformation that supports the collective hydrogen-bond network, the all-*anti* diastereomers can thermally access a large number of distinctly different backbone conformers at room temperature, each of which features its own structural dynamics related to the noncovalent OH···OH-contacts.

Let us now go back to Figure 12 (bottom panels) and inspect the experimental OH stretching infrared spectra of these polyols under ambient conditions. In the case of the all-*syn*-polyols, the OH stretching region is dominated by a broad, structureless, and strongly red-shifted band resulting from hydrogen-bonded hydroxy groups (δ-OH). Free OH groups are very weakly discernible only for the all-*syn*-diol around 3624 cm^{-1}. Importantly, the dominating δ resonance shifts markedly to lower frequencies with increasing network length. This behavior is perfectly reproduced by the DFT calculations and reminds us of the bathochromic shift of the lowest electronic transition of J-aggregates with increasing delocalization length of the exciton.[57] However, the experimental spectra of the polyols are highly broadened, having spectral bandwidths well in excess of 100 cm^{-1}. In light of the couplings of about 20 cm^{-1} between neighboring OH groups, it must be concluded that the stretching vibrational excitations are mostly localized on the individual hydroxy sites. Therefore, an "exchange" narrowing (as is typical for J-aggregates) is not observed for the vibrational resonances upon increasing the chain length.[56]

The infrared spectra of the all-*anti*-polyols greatly resemble the spectrum of ethanol oligomers with a pronounced δ band and a slightly weaker α/β peak. The splitting into two bands indicates that hydrogen bonding is still possible but also that it is indeed inhibited by the unfavorable stereochemistry. As opposed to the all-*syn*-polyols, a gradual shift to lower frequency with increasing chain length is not observed. This behavior is also reproduced in the DFT calculations, which reveal nearest neighbor couplings for the extended backbone conformers of no more than 10 cm^{-1}, that is, roughly half of the OH···OH interactions in the all-*syn* diastereomers.

The different coupling strengths obtained for corresponding diastereomers has an impact on the dynamics of both vibrational relaxation and vibrational spectral diffusion. In the left column of Figure 14, a series of 2DIR hole-burning

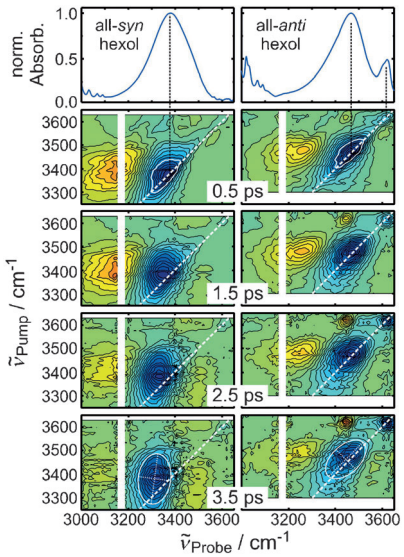

Figure 14. Two-dimensional infrared spectra of the all-*syn*- (left column) and all-*anti*-hexol (right column) in liquid $CDCl_3$ at room temperature recorded at various waiting delays. The top panels display the linear FTIR spectra of the two compounds.

spectra are shown for the all-*syn*-hexol together with its FTIR spectrum. At early waiting delays, a diagonally elongated ground-state hole/stimulated emission is seen. In addition, a diagonally stretched excited-state absorption is also observed and appears to be anharmonically shifted by about 200 cm^{-1}. Note that this value is similar to the anharmonicity of uncoupled local hydroxy oscillators, thereby signaling that despite of the favorable stereochemistry, the OH stretching excitations of the all-*syn*-hexol are predominantly local in character at room temperature.

As the waiting time is increased, the induced $v = 1 \rightarrow 2$ absorption decays (indicating vibrational relaxation) and the diagonal tilt vanishes (indicating spectral homogenization). The transition from an inhomogeneously broadened 2DIR line shape at early waiting delays to a homogeneously broadened one at later delays is further emphasized by the ellipse added to the 2DIR spectrum at 3.5 ps, whose long principal axis is aligned mostly parallel to the pump-frequency axis. Furthermore, the form of the contours of the 2DIR bleaching/emission peak at early waiting times is highly

interesting. Spectral holes burned into the high frequency wing of the OH stretching band (say at 3450 cm^{-1}) appear to be much broader than those burned into the low-frequency wing (e.g. at 3300 cm^{-1}). This behavior is highlighted by the white contour representing the pump and probe frequency pairs, where the differential optical density has decayed by a factor of two relative to the maximal bleaching/emission signal located on the diagonal at $\nu_{Pump} = \nu_{Probe} = 3380\ cm^{-1}$. It can be seen that this 50% contour has the peculiar shape of a semicircle that is titled by 45°. The arc of the semicircle extends well into the spectral region to the left of the diagonal while its base closely follows the diagonal. The appearance of the contours can be understood in light of the results discussed in Section 4.

From systems with two coupled hydroxy groups, such as DHN, we have learned that a pair of bleaching cross-peaks is to be expected and which appears promptly with the laser excitation. However, it was also noticed (see Figures 5 and 6) that one of these cross-peaks (namely δ_X, that is, pumping δ-OH and probing α-OH) is concealed by an absorptive transition (δ_C) from the pumped δ-OH fundamental to the combination level. In the case of an assembly of a larger number N of coupled OH oscillators, the vibrational manifold consists of a ground state, N fundamental states bearing one quantum of excitation (one-exciton states), and $N(N+1)/2$ states with two vibrational quanta (two-exciton states). The latter set of levels is composed of N overtone states bearing two quanta in the same mode and $N(N-1)/2$ combination states bearing two quanta in different modes.

Assuming the N site frequencies to be statically distributed across the linear OH stretching band, the 2DIR spectrum in the fundamental region of the assembly will feature N diagonal peaks and $N(N-1)$ cross-peaks. As well as these N^2 bleaching/emission signals, there will be $N^2(N+1)/2$ absorptive signals, namely, N transitions from the fundamentals to their overtones states, $N(N-1)$ allowed, and $N^2(N-1)/2$ forbidden transitions from the fundamentals to the combination tones. Provided the local anharmonicities are much larger than the site-frequency splittings, which in turn are smaller than the couplings, the set of fundamental cross-peaks and the set of allowed absorptions from the one-exciton manifold to the combination levels will largely cancel each other in the spectral region below the diagonal of the 2DIR spectrum (i.e. where $\nu_{probe} > \nu_{pump}$). Since such cancellation effects do not happen for $\nu_{probe} < \nu_{pump}$, the $v = 0 \rightarrow 1$ region of the 2DIR spectrum becomes asymmetrically distorted with respect to the diagonal. In the presence of dynamical line broadening, cross- and diagonal peaks will strongly overlap and will ultimately merge into a single unresolved bleaching/emission peak that decays much more rapidly below the diagonal than above.

The temporal evolution of the 2DIR spectrum of the all-*anti* hexol is displayed in the right column of Figure 14. Focusing first on the data taken at a waiting delay of 500 fs, it can be noticed that the spectral holes burned into the δ-OH resonance of the all-*anti*-hexol are much narrower than those of the all-*syn*-hexol. We can attribute this finding directly to the diminished couplings between adjacent hydroxy groups in reversing the stereochemical arrangement of the OH groups from 1,3-*syn* to 1,3-*anti*. In the limit of vanishing couplings, no fundamental cross-peak would survive. Although not as pronounced as before, the asymmetric shape of the 2DIR contours with respect to the diagonal is nonetheless discernible in the unfavorable stereochemistry. Disregarding the presence of the α-OH resonance, the two sets of 2DIR spectra are strikingly different in their line-broadening dynamics. Whereas the fundamental region of the all-*syn*-hexol is completely homogenized after 3.5 ps, the bleaching/emission peak of the all-*anti* diastereomers remains diagonally tilted (cf. white ellipse). This long-lived inhomogeneity is a direct consequence of the conformational diversity of the hydrocarbon backbone when the OH groups are improperly configured and is revealed as such by the 2DIR data only because transitions between different backbone conformers are slow compared to the OH stretching vibrational lifetimes.

This brings us to the dynamics of the vibrational relaxation of the networks. Figure 14 demonstrates that the anharmonically shifted absorption decays within a few ps because of the finite lifetime τ_{vib} of the $v = 1$ states. It seems that the all-*anti*-hexol features a slightly longer lifetime than its all-*syn* counterpart, which is in agreement with the findings presented above on the simpler diols that vibrational relaxation accelerates upon hydrogen bonding. Since the all-*anti*-polyols feature weaker hydrogen bonds than all-*syn*-polyols, there even seems to be a direct correlation between the strength of the noncovalent contact and the $v = 1$ lifetime. From what we have learned in Section 2 regarding the correlation between the OH stretching frequency and the hydrogen-bond geometry, we are led to raise the question of whether or not it is even possible to quantify this correlation by measuring the vibrational lifetime as a function of the pump frequency. The time-dependent 2DIR spectra enable us to do exactly this, namely, by plotting as a function of time the pump-induced optical density—integrated over the probe-frequency window covering the excited state absorption—for a variety of selected pump frequencies. Representative results of such an analysis are collected in Figure 15 for the two diastereomeric hexols. A complementary analysis for the tetrols was previously published in Ref. [55b].

It can be seen that the decay of the $v = 1$ induced absorption of the all-*syn*-polyol depends only weakly on the pump frequency. Tuning the pump pulse all the way through the resonance causes τ_{vib} to change by no more than 30%. Thus, the vibrational relaxation dynamics appear almost homogeneous with respect to the excitation frequency. In contrast, the vibrational lifetime of the all-*anti*-polyol is a highly sensitive function of the spectral position of the pump pulse within the OH stretching absorption band. More precisely, τ_{vib} decreases from 1.8 ps to 0.8 ps (i.e. by more than a factor of two) when tuning the excitation pulse from the high to the low-frequency edge of the resonance. Therefore, the dynamics of vibrational relaxation appear heterogeneous with regard to the excitation frequency. This totally distinct behavior of the two diastereomeric alcohols can again be rationalized by the different inter-hydroxy couplings.

Above, it was concluded that in solution at room temperature, the OH stretching excitation should be considered as being localized on individual OH groups regardless of the

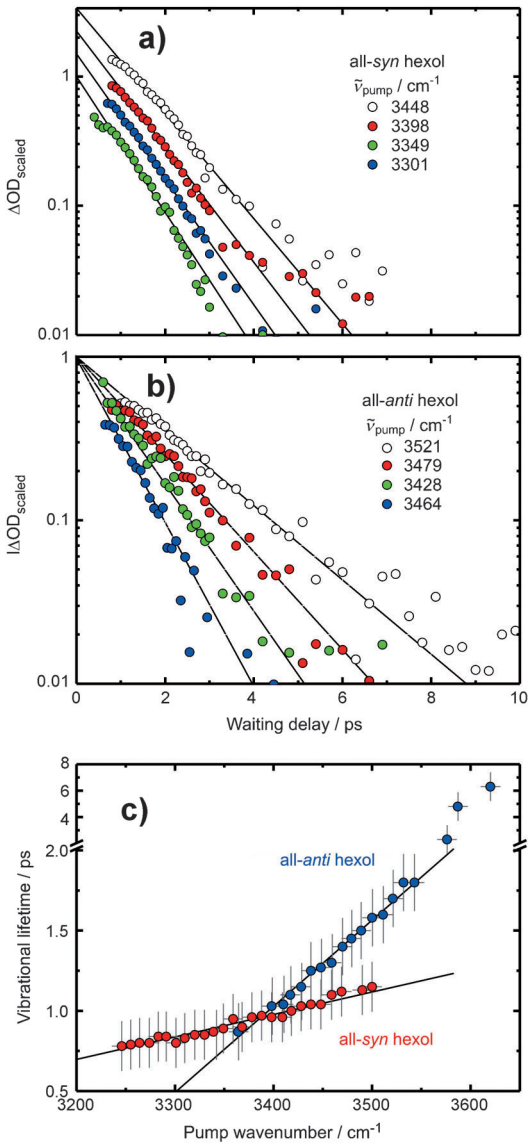

Figure 15. Decay of the excited-state absorption v = 1 as a function of the pump frequency for the all-*syn*- (a) and the all-*anti*-hexol (b) in a semilogarithmic representation. c) OH stretching vibrational lifetime as a function of the pump frequency.

stereochemistry. The hopping time, that is, the average time it takes the excitation to jump from one local hydroxy site to another, can be crudely estimated from the coupling β through Fermi's golden rule of $\tau_{hop} = (k_B T/h)/(2\pi c\beta)^2$, where k_B denotes Boltzmann's constant, h is Planck's constant, and c is the speed of light. Using the DFT results for the couplings and a temperature T of 300 K, the vibrational excitation can be expected to reside on an individual OH vibrator for about 440 fs in the all-*syn*-polyols or for roughly 1.8 ps in the all-*anti* diastereomers. Thus, depending on the stereochemical arrangement of the OH groups, excitation hopping within the $v = 1$ OH stretching manifold may or may not efficiently compete with vibrational energy relaxation and recovery of the $v = 0$ ground state. In addition, our notion of 2DIR hole burning may break down simply because the vibrational excitation can substantially randomize among all the OH groups constituting the hydrogen-bonded chain even within the duration of the narrow-band (and, hence, temporally long) pump pulse. In simple terms, heterogeneous relaxation dynamics are observed for all-*anti*-polyols because the inter-hydoxy couplings are small and the residence time of the excitation on a local site is long. As a result, the narrow-band pump can photoselect from the inhomogeneously broadened resonance a sub-ensemble of OH oscillators, each of which relaxes with its own unique vibrational lifetime. Accordingly, narrow-band ground-state holes arise in the 2DIR spectrum at early waiting delays. In contrast, homogeneous relaxation dynamics are observed for all-*syn*-polyols because the inter-hydroxy couplings are large and the residence time is short. Consequently, the narrow-band pump is no longer able to photoselect individual OH oscillators and broad-band ground-state holes are seen in the early 2DIR spectrum. In the limiting case where the vibrational couplings are much larger than the local OH stretching relaxation rates, the 2DIR experiment gives a canonically averaged vibrational lifetime that should be entirely independent of the excitation frequency. The averaging is caused by rapid OH stretching excitation hopping as described above—a process that is formally equivalent to intraband relaxation in electronic aggregates.

Finally, the mechanism of vibrational relaxation needs to be discussed. The series of 2DIR spectra (cf. Figure 14) display a characteristic absorption that is shifted to higher probe frequencies compared to the diagonal bleach/emission signal and whose amplitude grows with increasing waiting delay. The gradual appearance of a blue-shifted absorption indicates that vibrational relaxation leaves the hydrogen-bonded network in a heavily perturbed state with weaker and longer noncovalent contacts. When integrating the 2DIR spectrum at 3.5 ps over the pump-frequency axis, a conventional pump-probe spectrum can be calculated (projection slice theorem).[24b] It turns out that this projected spectrum matches a thermal difference spectrum that can be independently obtained by subtracting two FTIR spectra recorded at different temperatures. The correspondence between these two different types of spectra provides strong evidence that the pump-induced excess OH stretching vibrational energy is fully redistributed among all the vibrational degrees of freedom of the molecules in a canonical fashion. The resultant temperature jump can be crudely estimated using the harmonic frequencies from the DFT calculation. A 3400 cm^{-1} photon thus raises the vibrational temperature of the tetrols by about 80 K and of the hexols by about 60 K. The question then is: how can the vibrational energy redistribute so rapidly?

One mechanism originally proposed by Staib and Hynes[61] for vibrational energy relaxation in hydrogen-bonded dimers is based on a predissociation mechanism in which the OH stretching energy is effectively dumped into the O···O stretching coordinate of the dimer (see section 2). The flow of energy from the high-frequency intramolecular mode to the low-frequency intermolecular mode is facilitated by a non-adiabatic coupling between the $v = 1$ OH stretching state initially prepared by the pump photon and the O···O "translational" continuum associated with the $v = 0$ OH

stretching ground state where the dimer can ultimately break apart. Such a predissociation is possible because the binding energy of the dimer on the adiabatic $v=0$ potential energy surface is lower than the photon energy (ca. 3400 cm^{-1}) that is used to resonantly drive the intramolecular OH stretching fundamental with an infrared pulse at time zero. In our polyalcohols, an O···O "translational" continuum cannot exist because the hydrogen-bonded chain is supported by a hydrocarbon backbone that prevents the hydroxy groups from falling apart completely. However, the OH stretching coordinate may also couple to the low-frequency CC-OH torsional degrees of freedom. The torsional barriers are significantly smaller than average OH stretching frequency and, therefore, breakage of a hydrogen bond through the CC-OH torsional continuum following a non-adiabatic transition between $v=0$ and $v=1$ is energetically feasible. Unfortunately, such a mechanism has not yet been explored theoretically. The original predissociation model utilized the analytical Lippincott–Schroeder potential energy function[62] to quantify the predissociation rate for a general hydrogen-bonded dimer and, therefore, considered only the coupling between the high-frequency OH stretch and the low-frequency O···O stretch. Furthermore, it even predicted a dependence of the vibrational lifetime on the frequency of the pump pulse, as seen in Figure 15, because the less vibrational energy that has to be transferred to translational degrees of freedom, the more efficient becomes the breakage of the hydrogen bond. However, for oligomers of aliphatic alcohols dissolved in nonpolar solvents, the theory yielded inverse predissociation rates that were about an order of magnitude smaller than the vibrational lifetimes reported by several experimental groups.[52d,f,g]

Kwac and Geva studied the hydrogen-bonded structure and dynamics of methanol oligomers in liquid CCl_4 solutions by means of more sophisticated mixed quantum-classical molecular dynamics simulations.[63] The hydroxy stretching coordinate was treated fully quantum mechanically, while the remaining degrees of freedom were treated classically. The infrared spectrum was computed by on-the-fly diagonalization of the adiabatic Hamiltonian to obtain the time-dependent energy gap between the OH stretching ground and fundamental states. In addition, a vibrational lifetime was calculated from a Fermi's golden rule rate constant for the nonradiative transition from the first excited state to the ground state, which compares quite well with the experimental OD stretch lifetime of deuterated ethanol oligomers in CCl_4 solution. Unfortunately, the role of a mid-IR-induced predissociation of the hydrogen bond in the relaxation of vibrational energy within chains of hydrogen-bonded hydroxy oscillators has not been further explored in these studies.

Finally, a highly intriguing concept of vibrational energy relaxation in hydrogen-bonded systems was very recently put forth by Hamm and Stock,[64] who stressed the equivalence between electronic and vibrational relaxation dynamics when true crossings of adiabatic (electronic or vibrational) potential energy surfaces occur. Such vibrational conical intersections may arise upon coupling two high-frequency modes (such as OH stretches or COH bendings) with a minimum of two low-frequency modes (such as hydrogen-bond stretches or bendings or CC-OH torsions). In this picture, the ultrashort mid-infrared laser pulse drives the fundamental transition of one of the high-frequency modes and launches a nuclear wave packet in its first excited state. The motion of the wave packet is directed along the low-frequency coordinates and takes place on the two coupled adiabatic surfaces representing the two fundamental states in the high-frequency vibrational coordinates. Thus, the population in the initially prepared excited state can be efficiently funneled through the conical interactions to the energetically lower lying high-frequency fundamental. Figure 8d gives an example where the existence of a conical intersection between two high-frequency OH stretches (the α- and δ-OH of a diol) can be predicted by virtue of their coupling to the two low-frequency CC-OH torsions that facilitate their dynamical exchange through hydrogen-bond flip-flop. It would be interesting to explore the dependence of the adiabatic ground state and the excited COH bending states on these two torsional degrees of freedom to test whether or not additional conical intersections can ultimately funnel the initial OH stretching vibrational energy fully into kinetic energy of the low-frequency modes. Hamm and Stock have derived model parameters for malonaldehyde as a model system featuring a single hydrogen-bonded hydroxy group only and have shown that subpicosecond OH stretching vibrational lifetimes are indeed made possible by conical intersections. It remains to be seen whether or not such non-adiabatic wave packet dynamics are indeed responsible for the ultrafast vibrational relaxation seen in the extended hydrogen-bond networks discussed above. We are currently in the process of constructing adiabatic potential energy surfaces for the simple diols in an effort to identify the low-frequency coordinates that bring about vibrational conical intersections that bring about vibrational conical intersections serving as efficient mid-infrared photochemical funnels for vibrational energy.

7. Summary and Prospects

This Review has focused mostly on the 2DIR method and applications to very simple hydrogen-bonded systems. We started out from a simple diol featuring a single hydrogen bond between two weakly coupled hydroxy groups and a diol having its two OH groups fully decoupled. We have seen that the 2DIR spectra can reveal not only the couplings between the two interacting groups but also their individual anharmonicities. These are important quantities that can be used, for example, for testing or even benchmarking high-level electronic structure calculations on systems containing hydrogen bonds. We have also come across highly complex molecular dynamical processes, in particular structural rearrangements occurring at thermal equilibrium, that are revealed as chemical exchange in the time-dependent 2DIR spectra. Furthermore, structural fluctuations within a continuous distribution of hydrogen-bonded configurations lead to spectral diffusion and are seen in the dynamic evolution of 2DIR peak shapes. We closed with extended but finite size hydrogen-bond networks whose dynamics were controlled by chemical means. Depending on the strength of the couplings between

neighboring groups and the structural disorder of the network, vibrational excitations can be fully delocalized or they can incoherently hop between the structural units. Excitation transfer may compete efficiently with energy relaxation, thus giving rise to a distribution of vibrational lifetimes across the linear absorption band. All of these highly diverse phenomena will of course also occur in the random network of liquid water. Some of these have indeed been discovered, others remain obscured because of the infinite size of the liquid's network. Our understanding of the molecular dynamics in liquid water has tremendously advanced during the last few years thanks to fs-2DIR spectroscopy. In the context of hydrogen bonding, the technique continues to be pushed forward both in terms of methodology and in terms of applications. As examples we mention only briefly the development of surface-sensitive 2DIR spectroscopy through sum-frequency generation and its application to aqueous lipid-membrane interfaces[65] or higher-order multidimensional spectroscopy with sequences of ultrafast IR laser pulses to reveal heterogeneous dynamics in bulk liquid water.[66] Hydrogen-bond networks are ubiquitous and play a fundamental role in biochemical systems and in systems of technological relevance. There is still a wide range of open questions related to hydrogen bonding, where 2DIR spectroscopy will leave its important footprints.

We thank all former co-workers and collaborators of the Vöhringer Group who were engaged in this research. Financial support by the German Science Foundation through the Collaborative Research Centers 813 "Chemistry at Spin Centers" and 624 "Functional Chemical Templates" is gratefully acknowledged.

Received: December 14, 2012
Published online: July 10, 2013

[1] J.-P. Hansen, I. R. McDonald, *Theory of simple liquids*, *3rd ed.*, Academic Press, London, **2009**.
[2] C. G. Maitland, M. Rigby, E. B. Smith, W. A. Wakeham, *Intermolecular forces—their origin and determination*, Clarendon, Oxford, **1981**.
[3] H. C. Andersen, *Annu. Rev. Phys. Chem.* **1975**, *26*, 145–166.
[4] a) G. C. Pimentel, A. L. McClellan, *The hydrogen bond*, W. H. Freeman, San Francisco, **1960**; b) G. A. Jeffrey, *An intrduction to hydrogen bonding*, Oxford University Press, New York, **1997**; c) S. J. Grabowski, *Hydrogen Bonding—New Insights*, *Vol. 3*, Springer, Amsterdam, **2006**.
[5] a) K. Laasonen, M. Sprik, M. Parrinello, R. Car, *J. Chem. Phys.* **1993**, *99*, 9080–9089; b) C. Cavazzoni, G. L. Chiarotti, S. Scandolo, E. Tosatti, M. Bernasconi, M. Parrinello, *Science* **1999**, *283*, 44–46; c) D. Marx, M. E. Tuckerman, J. Hutter, M. Parrinello, *Mol. Phys.* **1999**, *397*, 601–604; d) P. L. Geissler, C. Dellago, D. Chandler, J. Hutter, M. Parrinello, *Science* **2001**, *291*, 2121–2124; e) I. F. W. Kuo, C. J. Mundy, M. J. McGrath, J. I. Siepmann, *J. Chem. Theory Comput.* **2006**, *2*, 1274–1281; f) F. Paesani, G. A. Voth, *J. Phys. Chem. B* **2009**, *113*, 5702–5719.
[6] a) F. H. Stillinger, *Int. J. Quant. Chem.* **1978**, *14*, 649–657; b) M. L. Klein, I. R. McDonald, *J. Chem. Phys.* **1979**, *71*, 298–308; c) R. W. Impey, M. L. Klein, *Chem. Phys. Lett.* **1984**, *104*, 579–582; d) B. M. Ladanyi, M. S. Skaf, *Annu. Rev. Phys. Chem.* **1993**, *44*, 335–368; e) K. B. Lipkowitz, D. B. Boyd, A. Wallqvist, R. D. Mountain, *J. Comp. Chem.* **2007**, *13*, 183–247.
[7] a) D. Eisenberg, W. Kauzmann, *The structure and the properties of water*, Oxford University Press, Oxford, **1969**; b) F. Franks in *Water*, *A comprehensive treatise*, *Vol. 1* (Ed.: F. Franks), Plenum Press, New York, **1972**; c) F. H. Stillinger, *Science* **1980**, *209*, 451–457; d) R. Ludwig, *Angew. Chem.* **2001**, *113*, 1856–1876; *Angew. Chem. Int. Ed.* **2001**, *40*, 1808–1827; e) Y. Maréchal, *The hydrogen-bond and the water molecule*, Elsevier, Amsterdam, **2007**.
[8] a) A. H. Narten, H. A. Levy, *J. Chem. Phys.* **1971**, *55*, 2263–2269; b) A. K. Soper, M. G. Phillips, *Chem. Phys.* **1986**, *107*, 47–60; c) A. K. Soper, F. Bruni, M. A. Ricci, *J. Chem. Phys.* **1997**, *106*, 247–254; d) G. Hura, J. M. Sorenson, R. M. Glaeser, T. Head-Gordon, *J. Chem. Phys.* **2000**, *113*, 9140–9148; e) J. M. Sorenson, G. Hura, R. M. Glaeser, T. Head-Gordon, *J. Chem. Phys.* **2000**, *113*, 9149–9161; f) P. Wernet, D. Nordlund, U. Bergmann, M. Cavalleri, M. Odelius, H. Ogasawara, L. Å. Näslund, T. K. Hirsch, L. Ojamäe, P. Glatzel, L. G. M. Pettersson, A. Nilsson, *Science* **2004**, *304*, 995–999.
[9] See Ref. [8e].
[10] a) C. J. Montrose, J. A. Bucaro, J. Mashall-Coakley, T. A. Litowitz, *J. Chem. Phys.* **1974**, *60*, 5025–5029; b) O. Conde, J. Teixeira, *J. Phys.* **1983**, *44*, 525–529.
[11] J. Teixeira, M. C. Bellissent-Funel, S. H. Chen, *J. Phys. Condens. Matter* **1990**, *2*, Sa105–Sa108.
[12] G. Sposito, *J. Chem. Phys.* **1981**, *74*, 6943–6949.
[13] N. Agmon, *Chem. Phys. Lett.* **1995**, *244*, 456–462.
[14] G. R. Fleming, M. Cho, *Annu. Rev. Phys. Chem.* **1996**, *47*, 109–134.
[15] T. Elsaesser, H. J. Bakker, *Ultrafast Hydrogen Bonding Dynamics and Proton Transfer Processes in the Condensed Phase*, Kluwer, Dordrecht, **2003**.
[16] a) H. K. Nienhuys, R. A. van Santen, H. J. Bakker, *J. Chem. Phys.* **2000**, *112*, 8487–8494; b) H. J. Bakker, Y. L. A. Rezus, R. L. A. Timmer, *J. Phys. Chem. A* **2008**, *112*, 11523–11534.
[17] a) M. F. Kropman, H. K. Nienhuys, S. Woutersen, H. J. Bakker, *J. Phys. Chem. A* **2001**, *105*, 4622–4626; b) H. J. Bakker, H. K. Nienhuys, G. Gallot, N. Lascoux, G. M. Gale, J. C. Leicknam, S. Bratos, *J. Chem. Phys.* **2002**, *116*, 2592–2598; c) A. J. Lock, H. J. Bakker, *J. Chem. Phys.* **2002**, *117*, 1708–1713; d) J. Lindner, P. Vöhringer, M. S. Pshenichnikov, D. Cringus, D. A. Wiersma, M. Mostovoy, *Chem. Phys. Lett.* **2006**, *421*, 329–333; e) D. Schwarzer, J. Lindner, P. Vöhringer, *J. Phys. Chem. A* **2006**, *110*, 2858–2867; f) S. Ashihara, N. Huse, A. Espagne, E. T. J. Nibbering, T. Elsaesser, *J. Phys. Chem. A* **2007**, *111*, 743–746; g) L. Chieffo, J. Shattuck, J. J. Amsden, S. Erramilli, L. D. Ziegler, *Chem. Phys.* **2007**, *341*, 71–80; h) R. Rey, F. Ingrosso, T. Elsaesser, J. T. Hynes, *J. Phys. Chem. A* **2009**, *113*, 8949–8962; i) T. Schäfer, J. Lindner, P. Vöhringer, D. Schwarzer, *J. Chem. Phys.* **2009**, *130*, 224502–224508.
[18] a) M. L. Cowan, B. D. Bruner, N. Huse, J. R. Dwyer, B. Chugh, E. T. J. Nibbering, T. Elsaesser, R. J. D. Miller, *Nature* **2005**, *434*, 199–202; b) J. Lindner, D. Cringus, M. S. Pshenichnikov, P. Vöhringer, *Chem. Phys.* **2007**, *341*, 326–335.
[19] S. Woutersen, H. J. Bakker, *Nature* **1999**, *402*, 507–509.
[20] a) S. Woutersen, H. J. Bakker, *Phys. Rev. Lett.* **1999**, *83*, 2077–2080; b) C. J. Fecko, J. D. Eaves, J. J. Loparo, A. Tokmakoff, P. L. Geissler, *Science* **2003**, *301*, 1698–1702; c) D. Schwarzer, J. Lindner, P. Vöhringer, *J. Chem. Phys.* **2005**, *123*, 161105; d) J. J. Loparo, S. T. Roberts, A. Tokmakoff, *J. Chem. Phys.* **2006**, *125*, 194521; e) D. Kraemer, M. L. Cowan, A. Paarmann, N. Huse, E. T. J. Nibbering, T. Elsaesser, R. J. D. Miller, *Proc. Natl. Acad. Sci. USA* **2008**, *105*, 437–442.
[21] a) T. Steinel, J. B. Asbury, J. R. Zheng, M. D. Fayer, *J. Phys. Chem. A* **2004**, *108*, 10957–10964; b) C. J. Fecko, J. J. Loparo,

S. T. Roberts, A. Tokmakoff, *J. Chem. Phys.* **2005**, *122*, 054506; c) see Ref. [20d].

[22] a) R. Rey, J. T. Hynes, *J. Chem. Phys.* **1996**, *104*, 2356 – 2368; b) C. P. Lawrence, J. L. Skinner, *J. Chem. Phys.* **2002**, *117*, 5827 – 5838; c) C. P. Lawrence, J. L. Skinner, *J. Chem. Phys.* **2002**, *117*, 8847 – 8854; d) R. Rey, K. B. Møller, J. T. Hynes, *J. Phys. Chem. A* **2002**, *106*, 11993 – 11996; e) J. B. Asbury, T. Steinel, C. Stromberg, S. A. Corcelli, C. P. Lawrence, J. L. Skinner, M. D. Fayer, *J. Phys. Chem. A* **2004**, *108*, 1107 – 1119; f) C. P. Lawrence, J. L. Skinner, *Chem. Phys. Lett.* **2003**, *369*, 472 – 477; g) C. P. Lawrence, J. L. Skinner, *J. Chem. Phys.* **2003**, *119*, 3840 – 3848; h) K. B. Møller, R. Rey, J. T. Hynes, *J. Phys. Chem. A* **2004**, *108*, 1275 – 1289; i) R. Rey, K. B. Møller, J. T. Hynes, *Chem. Rev.* **2004**, *104*, 1915 – 1928; j) D. Laage, J. T. Hynes, *Science* **2006**, *311*, 832 – 835; k) D. Laage, J. T. Hynes, *J. Phys. Chem. B* **2008**, *112*, 14230 – 14242; l) H. J. Bakker, J. L. Skinner, *Chem. Rev.* **2010**, *110*, 1498 – 1517; m) C. Falvo, B. Palmieri, S. Mukamel, *J. Chem. Phys.* **2009**, *130*, 184501; n) A. Paarmann, T. Hayashi, S. Mukamel, R. J. D. Miller, *J. Chem. Phys.* **2009**, *130*, 204110 – 204113; o) T. L. C. Jansen, B. M. Auer, M. Yang, J. L. Skinner, *J. Chem. Phys.* **2010**, *132*, 224503.

[23] a) E. T. J. Nibbering, T. Elsaesser, *Chem. Rev.* **2004**, *104*, 1887 – 1914; b) S. T. Roberts, K. Ramasesha, A. Tokmakoff, *Acc. Chem. Res.* **2009**, *42*, 1239 – 1249.

[24] a) M. Cho, *Two-dimensional optical spectroscopy*, CRC, Boca Raton, **2009**; b) P. Hamm, M. T. Zanni, *Concepts and Methods of 2D Infrared Spectroscopy*, Cambridge University Press, Cambridge, **2011**.

[25] a) S. Rybak, B. Jeziorski, K. Szalewicz, *J. Chem. Phys.* **1991**, *95*, 6576 – 6601; b) K. Kim, K. D. Jordan, *J. Phys. Chem.* **1994**, *98*, 10089 – 10094; c) S. S. Xantheas, *J. Chem. Phys.* **1996**, *104*, 8821 – 8824; d) W. Klopper, J. G. C. M. van Duijneveldt-van de Rijdt, F. B. van Duijneveldt, *Phys. Chem. Chem. Phys.* **2000**, *2*, 2227 – 2234; e) G. S. Tschumper, M. L. Leininger, B. C. Hoffman, E. F. Valeev, H. F. Schaefer, M. Quack, *J. Chem. Phys.* **2002**, *116*, 690 – 701.

[26] It should be noted that the vibrational zero-point energy of $D_2O\cdots HOD$ is slightly higher than that of $D_2O\cdots DOH$. The energy difference is roughly 65 cm^{-1} (RI-MP2/def2-TZVPP). Therefore, strictly speaking, the chosen dimer configuration represents a local and not a global energy minimum. However, this issue does not affect the general discussion and conclusions drawn from this model system.

[27] H. G. Kjaergaard, A. L. Garden, G. M. Chaban, R. B. Gerber, D. A. Matthews, J. F. Stanton, *J. Phys. Chem. A* **2008**, *112*, 4324 – 4335.

[28] a) W. S. Benedict, N. Gailar, E. K. Plyler, *J. Chem. Phys.* **1956**, *24*, 1139 – 1165; b) L. Fredin, B. Nelander, G. Ribbegard, *J. Chem. Phys.* **1977**, *66*, 4065 – 4072.

[29] a) E. H. T. Olthof, A. van der Avoird, P. E. S. Wormer, J. G. Loeser, R. J. Saykally, *J. Chem. Phys.* **1994**, *101*, 8443 – 8454; b) K. Liu, J. D. Cruzan, R. J. Saykally, *Science* **1996**, *271*, 929 – 933; c) T. Häber, U. Schmitt, M. A. Suhm, *Phys. Chem. Chem. Phys.* **1999**, *1*, 5573 – 5582; d) F. N. Keutsch, R. J. Saykally, *Proc. Natl. Acad. Sci. USA* **2001**, *98*, 10533 – 10540; e) R. W. Larsen, P. Zielke, M. A. Suhm, *J. Chem. Phys.* **2007**, *126*, 194307; f) M. A. Suhm, *Adv. Chem. Phys.* **2009**, *142*, 1 – 57; g) T. N. Wassermann, M. A. Suhm, *J. Phys. Chem. A* **2010**, *114*, 8223 – 8233.

[30] a) M. N. Afsar, J. B. Hasted, *J. Opt. Soc. Am.* **1977**, *67*, 902 – 904; b) M. N. Afsar, J. B. Hasted, *Infrared Phys.* **1978**, *18*, 835 – 841.

[31] a) J. T. Kindt, C. A. Schmuttenmaer, *J. Chem. Phys.* **1997**, *106*, 4389 – 4400; b) M. Heyden, J. Sun, S. Funkner, G. Mathias, H. Forbert, M. Havenith, D. Marx, *Proc. Natl. Acad. Sci. USA* **2010**, *107*, 12068 – 12073.

[32] G. E. Walrafen, *J. Phys. Chem.* **1990**, *94*, 2237 – 2239.

[33] a) K. Winkler, J. Lindner, H. Bürsing, P. Vöhringer, *J. Chem. Phys.* **2000**, *113*, 4674 – 4682; b) K. Winkler, J. Lindner, P. Vöhringer, *Phys. Chem. Chem. Phys.* **2002**, *4*, 2144 – 2155.

[34] A. Kandratsenka, D. Schwarzer, P. Vöhringer, *J. Chem. Phys.* **2008**, *128*, 244510 – 244516.

[35] S. Mukamel, *Principles of nonlinear optical spectroscopy*, Oxford University Press, New York, **1995**.

[36] It is important to emphasize that in a real molecular liquid the frequency–structure correlations are much more complex than in the simple water dimer, where we have only considered the effect of the hydrogen-bond distance on the OH stretching resonance. Indeed, quite different local hydrogen-bond environments can lead to the same OH stretching frequency.

[37] J. T. Fourkas, *Annu. Rev. Phys. Chem.* **2002**, *53*, 17 – 40.

[38] The terms "absorbance" and "optical density" are synonymous. The optical density of a sample can be derived from the intensities of a transmitted and a reference beam of light according to the Lambert–Beer law.

[39] a) K. Lazonder, M. S. Pshenichnikov, D. A. Wiersma, *Opt. Lett.* **2006**, *31*, 3354 – 3356; b) S. T. Roberts, J. J. Loparo, A. Tokmakoff, *J. Chem. Phys.* **2006**, *125*, 084502.

[40] J. C. Owrutsky, D. Raftery, R. M. Hochstrasser, *Annu. Rev. Phys. Chem.* **1994**, *45*, 519 – 553.

[41] P. Hamm, M. H. Lim, R. M. Hochstrasser, *J. Phys. Chem. B* **1998**, *102*, 6123 – 6138.

[42] a) M. C. Asplund, M. T. Zanni, R. M. Hochstrasser, *Proc. Natl. Acad. Sci. USA* **2000**, *97*, 8219 – 8224; b) L. P. DeFlores, R. A. Nicodemus, A. Tokmakoff, *Opt. Lett.* **2007**, *32*, 2966 – 2968; c) J. Helbing, P. Hamm, *J. Opt. Soc. Am. B* **2011**, *28*, 171 – 178.

[43] V. Cervetto, J. Helbing, J. Bredenbeck, P. Hamm, *J. Chem. Phys.* **2004**, *121*, 5935 – 5942.

[44] a) S. H. Shim, M. T. Zanni, *Phys. Chem. Chem. Phys.* **2009**, *11*, 748 – 761; b) D. B. Strasfeld, S. H. Shim, M. T. Zanni, *Adv. Chem. Phys.* **2009**, *141*, 1 – 28.

[45] E. B. Wilson, Jr., J. C. Decius, P. C. Cross, *Molecular vibrations, The theory of infrared and Raman vibrational spectra*, McGraw-Hill, London, **1955**.

[46] a) H. Graener, G. Seifert, *J. Chem. Phys.* **1993**, *98*, 36 – 45; b) H. Graener, G. Seifert, A. Laubereau, *Chem. Phys.* **1993**, *175*, 193 – 204; c) T. L. C. Jansen, D. Cringus, M. S. Pshenichnikov, *J. Phys. Chem. A* **2009**, *113*, 6260 – 6265.

[47] a) W. Saenger, C. Betzel, B. Hingerty, G. M. Brown, *Nature* **1982**, *296*, 581 – 583; b) W. Saenger, C. Betzel, B. Hingerty, G. M. Brown, *Angew. Chem.* **1983**, *95*, 908 – 909; *Angew. Chem. Int. Ed. Engl.* **1983**, *22*, 883 – 884; c) J. E. H. Koehler, W. Saenger, W. F. Gunsteren, *Eur. Biophys. J.* **1988**, *16*, 153 – 168; d) M. Olschewski, J. Lindner, P. Vöhringer, *Angew. Chem.* **2013**, *125*, 2663 – 2667; *Angew. Chem. Int. Ed.* **2013**, *52*, 2602 – 2605.

[48] R. G. Gilbert, S. C. Smith, *Theory of Unimolecular and Recombination Reactions*, Blackwell Scientific, Oxford, **1990**.

[49] a) S. Woutersen, Y. Mu, G. Stock, P. Hamm, *Chem. Phys.* **2001**, *266*, 137 – 147; b) Y. S. Kim, R. M. Hochstrasser, *Proc. Natl. Acad. Sci. USA* **2005**, *102*, 11185 – 11190; c) J. Zheng, K. Kwak, J. Asbury, X. Chen, I. R. Piletic, M. D. Fayer, *Science* **2005**, *309*, 1338 – 1343; d) K. Kwak, J. Zheng, H. Cang, M. D. Fayer, *J. Phys. Chem. B* **2006**, *110*, 19998; e) J. F. Cahoon, K. R. Sawyer, J. P. Schlegel, C. B. Harris, *Science* **2008**, *319*, 1820 – 1823; f) M. D. Fayer, *Annu. Rev. Phys. Chem.* **2009**, *60*, 21 – 38.

[50] A. D. Bain, *Prog. Nucl. Magn. Reson. Spectrosc.* **2003**, *43*, 63 – 103.

[51] a) M. Quack, M. A. Suhm, *Chem. Phys. Lett.* **1990**, *171*, 517 – 524; b) M. Quack, M. A. Suhm, *J. Chem. Phys.* **1991**, *95*, 28 – 59; c) M. Quack, M. A. Suhm, *Chem. Phys. Lett.* **1991**, *183*, 187 – 194.

[52] a) H. Graener, T. Q. Ye, *J. Phys. Chem.* **1989**, *93*, 5963 – 5965; b) H. Graener, T. Q. Ye, A. Laubereau, *J. Chem. Phys.* **1989**, *91*, 1043 – 1046; c) H. Graener, T. Q. Ye, A. Laubereau, *J. Chem. Phys.* **1989**, *90*, 3413 – 3416; d) S. Woutersen, U. Emmerichs, H. J.

Bakker, *J. Chem. Phys.* **1997**, *107*, 1483 – 1490; e) N. E. Levinger, P. H. Davis, M. D. Fayer, *J. Chem. Phys.* **2001**, *115*, 9352 – 9360; f) K. J. Gaffney, P. H. Davis, I. R. Piletic, N. E. Levinger, M. A. Fayer, *J. Phys. Chem. A* **2002**, *106*, 12012 – 12023; g) K. J. Gaffney, I. R. Piletic, M. D. Fayer, *J. Phys. Chem. A* **2002**, *106*, 9428 – 9435.

[53] a) B. M. Auer, J. L. Skinner, *J. Chem. Phys.* **2008**, *128*, 224511 – 224512; b) A. Paarmann, T. Hayashi, S. Mukamel, R. J. D. Miller, *J. Chem. Phys.* **2008**, *128*, 191103 – 191105; c) M. Yang, J. L. Skinner, *J. Chem. Phys.* **2011**, *135*, 164505.

[54] a) I. Paterson, J. P. Scott, *Tetrahedron Lett.* **1997**, *38*, 7445 – 7448; b) I. Paterson, J. P. Scott, *J. Chem. Soc. Perkin Trans. 1* **1999**, 1003 – 1014.

[55] a) J. Seehusen, J. Lindner, D. Schwarzer, P. Vöhringer, *Phys. Chem. Chem. Phys.* **2009**, *11*, 8484 – 8495; b) S. Knop, T. L. Jansen, J. Lindner, P. Vöhringer, *Phys. Chem. Chem. Phys.* **2011**, *13*, 4641 – 4650.

[56] H. Fidder, J. Knoester, D. A. Wiersma, *J. Chem. Phys.* **1991**, *95*, 7880 – 7890.

[57] M. W. Parson, *Modern optical spectroscopy*, Springer, Berlin, **2007**.

[58] J. T. King, C. R. Baiz, K. J. Kubarych, *J. Phys. Chem. A* **2010**, *114*, 10590 – 10604.

[59] R. M. Hexter, *J. Chem. Phys.* **1960**, *33*, 1833 – 1841.

[60] A. Remorino, R. M. Hochstrasser, *Acc. Chem. Res.* **2012**, *45*, 1896 – 1905.

[61] A. Staib, J. T. Hynes, *Chem. Phys. Lett.* **1993**, *204*, 197 – 205.

[62] E. R. Lippincott, R. Schroeder, *J. Chem. Phys.* **1955**, *23*, 1099 – 1106.

[63] a) K. Kwac, E. Geva, *J. Phys. Chem. B* **2011**, *115*, 9184 – 9194; b) K. Kwac, E. Geva, *J. Phys. Chem. B* **2012**, *116*, 2856 – 2866.

[64] P. Hamm, G. Stock, *Phys. Rev. Lett.* **2012**, *109*, 173201.

[65] a) J. Bredenbeck, A. Ghosh, H. K. Nienhuys, M. Bonn, *Acc. Chem. Res.* **2009**, *42*, 1332 – 1342; b) J. A. Mondal, S. Nihonyanagi, S. Yamaguchi, T. Tahara, *J. Am. Chem. Soc.* **2010**, *132*, 10656 – 10657; c) W. Xiong, J. E. Laaser, R. D. Mehlenbacher, M. T. Zanni, *Proc. Natl. Acad. Sci. USA* **2011**, *108*, 20902 – 20907.

[66] a) S. Garrett-Roe, P. Hamm, *J. Chem. Phys.* **2008**, *128*, 104507 – 104513; b) S. Garrett-Roe, P. Hamm, *Acc. Chem. Res.* **2009**, *42*, 1412 – 1422; c) S. Garrett-Roe, F. Perakis, F. Rao, P. Hamm, *J. Phys. Chem. B* **2011**, *115*, 6976 – 6984.